

Pontryagin Differentiable Programming: An End-to-End Learning and Control Framework

Wanxin Jin Zhaoran Wang Zhuoran Yang Shaoshuai Mou
Purdue University Northwestern University Princeton University Purdue University
{wanxinjin, zhaoranwang}@gmail.com zy6@princeton.edu mous@purdue.edu

Abstract

This paper develops a Pontryagin Differentiable Programming (PDP) methodology, which establishes a unified framework to solve a broad class of learning and control tasks. The PDP distinguishes from existing methods by two novel techniques: first, we differentiate through Pontryagin’s Maximum Principle, and this allows to obtain the analytical derivative of a trajectory with respect to tunable parameters within an optimal control system, enabling end-to-end learning of dynamics, policies, or/and control objective functions; and second, we propose an auxiliary control system in the backward pass of the PDP framework, and the output of this auxiliary control system is the analytical derivative of the original system’s trajectory with respect to the parameters, which can be iteratively solved using standard control tools. We investigate three learning modes of the PDP: inverse reinforcement learning, system identification, and control/planning. We demonstrate the capability of the PDP in each learning mode on different high-dimensional systems, including multi-link robot arm, 6-DoF maneuvering quadrotor, and 6-DoF rocket powered landing.

1 Introduction

Many learning tasks can find their counterpart problems in control fields. These tasks both seek to obtain unknown aspects of a decision-making system with different terminologies compared below.

Table 1: Topic connections between control and learning (details presented in Section 2)

UNKNOWN IN A SYSTEM	LEARNING METHODS	CONTROL METHODS
Dynamics $\mathbf{x}_{t+1} = \mathbf{f}_{\theta}(\mathbf{x}_t, \mathbf{u}_t)$	Markov decision processes	System identification
Policy $\mathbf{u}_t = \pi_{\theta}(t, \mathbf{x}_t)$	Reinforcement learning (RL)	Optimal control (OC)
Control objective $J = \sum_t c_{\theta}(\mathbf{x}_t, \mathbf{u}_t)$	Inverse RL	Inverse OC

With the above connections, learning and control fields have begun to explore the complementary benefits of each other: control theory may provide abundant models and structures that allow for efficient or certificated algorithms for high-dimensional tasks, while learning enables to obtain these models from data, which are otherwise not readily attainable via classic control tools. Examples that enjoy both benefits include model-based RL [1, 2], where dynamics models are used for sample efficiency; and Koopman-operator control [3, 4], where via learning, nonlinear systems are lifted to a linear observable space to facilitate control design. Inspired by those, this paper aims to exploit the advantage of integrating learning and control and develop a unified framework that enables to solve a wide range of learning and control tasks, e.g., the challenging problems in Fig. 1.

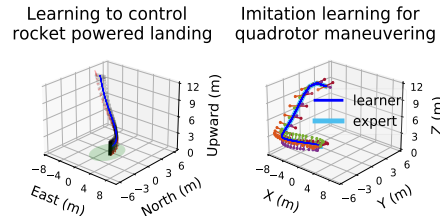


Figure 1: left: PDP learns rocket landing control, right: PDP learns quadrotor dynamics and control objective for imitation.

2 Background and Related Work

Learning dynamics. This is usually referred to as system identification in control fields, which typically consider linear systems represented by transfer functions [5]. For nonlinear systems, the Koopman theory [6] provides a way to lift states to a (infinite-dimensional) linear observable space [3, 7]. In learning, dynamics is characterized by Markov decision processes and implemented using linear regression [8], observation-transition modeling [9], latent-space modeling [10], (deep) neural networks [11], Gaussian process [12], transition graphs [13], etc. Although off-the-shelf, most of these methods have to trade off between data efficiency and long-term prediction accuracy. To achieve both, physically-informed learning [14–17] injects physics laws into learning models, but they are limited to mechanical systems. Recently, a trend of work starts to use dynamical systems to explain (deep) neural networks, and some new algorithms [18–25] have been established.

This paper focuses on learning general dynamical models, encompassing either physical dynamics with unknown parameters or neural difference equations. The proposed learning framework is injected with inductive knowledge of optimal control theory to achieve efficiency and explainability.

Learning optimal policies. In learning fields, it relates to reinforcement learning (RL). Model-free RL provides a general-purpose framework to learn policies directly from interacting with environments [26–28], but usually suffers from significant data complexity. Model-based RL addresses this by first learning a dynamics model from experience and then integrating it to policy improvement [1, 12, 29–31]. The use of a model can assist to augment experience data [32, 33], perform back-propagation through time [12], or test policies before deployment. Model-based RL also faces some challenges that are not well-addressed. For example, how to efficiently leverage imperfect models [34], and how to maximize the joint benefit by combining policy learning and motion planning (trajectory optimization) [31, 35], where a policy has the advantage of execution coherence and fast deployment while the trajectory planning has the competence of adaption to unseen or future situations.

The counterpart topic in control is optimal control (OC), which is more concerned with characterizing optimal trajectories in presence of dynamics models. As in RL, the main strategy for OC is based on dynamic programming, and many value-based methods are available, such as HJB [36], differential dynamical programming (DDP) [37] (by quadratizing dynamics and value function), and iterative linear quadratic regulator (iLQR) [38] (by linearizing dynamics and quadratizing value function). The second strategy to solve OC is based on the Pontryagin’s Maximum/Minimal Principle (PMP) [39]. Derived from calculus of variations, PMP can be thought of as optimizing directly over trajectories, thus avoiding solving for value functions. Popular methods in this vein include shooting methods [40] and collocation methods [41]. However, the OC methods based on PMP are essentially *open loop* control and thus susceptible to model errors or disturbances in deployment. To address these, model predictive control (MPC) [42] generates controls given the system current state by repeatedly solving an OC problem over a finite prediction horizon (only the first optimal input is executed), leading to a *closed-loop* control form. Although MPC has dominated across many industrial applications [43], developing fast MPC implementations is still an active research direction [44].

The proposed learning framework in this work has a special mode for model-based control tasks. The method can be viewed as a complement to classic open-loop OC methods, because, although derived from PMP (trajectory optimization), the method here is to learn a *feedback/closed-loop* control policy. Depending on the specific policy parameterization, the method here can also be used for motion planning. All these features will provide new perspectives for model-based RL or MPC control.

Learning control objective functions. In learning, this relates to inverse reinforcement learning (IRL), whose goal is to find a control objective function to explain the given optimal demonstrations. The unknown objective function is typically parameterized as a weighted sum of features [45–47]. Strategies to learn the unknown weights include feature matching [45] (matching the feature values between demonstrations and reproduced trajectories), maximum entropy [46] (finding a trajectory distribution of maximum entropy subject to empirical feature values), and maximum margin [47] (maximizing the margin of objective values between demonstrations and reproduced trajectories). The learning update in the above IRL methods is preformed on a selected feature space by taking advantage of linearity of feature weights, and thus cannot be directly applied to learning objective functions that are nonlinear in parameters. The counterpart topic in the control field is inverse optimal control (IOC) [48–51]. With knowledge of dynamics, IOC focuses on more efficient learning paradigms. For example, by directly minimizing the violation of optimality conditions by the observed demonstration data, [48, 50–52] directly compute feature weights without repetitively solving the OC problems.

Despite the efficiency, minimizing optimality violation does not directly assure the closeness between the final reproduced trajectory and demonstrations or the closeness of their objective values.

Fundamentally different from existing IRL/IOC methods, this paper will develop a new framework that enables to learn complex control objective functions, e.g., neural objective functions, by directly minimizing the loss (e.g., the distance) between the reproduced trajectory and demonstrations.

A unified perspective on learning dynamics/policy/control objective functions. Consider a general decision-making system, which typically consists of aspects of dynamics, control policy, and control objective function. In a unified perspective, learning dynamics, policies, or control objective functions can be viewed as *instantiations of the same learning problem* but with (i) unknown parameters appearing in the system’s different aspects and (ii) the different losses. For example, in learning dynamics, a differential/difference equation is parameterized and the loss function can be defined as the prediction error between the equation’s output and target data; in learning policies, the unknown parameters are in a feedback policy and the loss function is just the control objective function; and in learning control objective functions, the control objective function is parameterized and the loss function can be the discrepancy between the reproduced trajectory and the observed demonstrations.

Claim of contributions. Motivated by the above, this paper develops a unified learning framework, named as PDP, that is flexible enough to be customized for different learning and control tasks and capable enough to efficiently solve high-dimensional and continuous-space problems. The proposed PDP framework borrows the idea of ‘end-to-end’ learning [53] and chooses to optimize a loss function directly with respect to the tunable parameters in the aspect(s) of a decision-making system, such as the dynamics, policy, or/and control objective function. The key contribution of the PDP is that we inject the optimal control theory as an inductive bias into the learning process to expedite the learning efficiency and explainability. Specifically, the PDP framework centers around the system’s trajectory and *differentiates through PMP*, and this allows us to obtain the analytical derivative of the trajectory with respect to the tunable parameters, a key quantity for end-to-end learning of (neural) dynamics, (neural) policies, and (neural) control objective functions. Furthermore, we introduce an *auxiliary control system* in the back pass of the PDP framework, and its output trajectory is exactly the derivative of the trajectory with respect to the parameters, which can be iteratively solved using standard control tools. In control fields, to our best knowledge, this is the first work to propose the technique of the *differential PMP*, and more importantly, we show that the *differential PMP* can be easily obtained using the introduced auxiliary control system.

3 Problem Formulation

We begin with formulating a base problem and then discuss how to accommodate the base problem to specific applications. Consider a class of optimal control systems $\Sigma(\theta)$, which is parameterized by a tunable $\theta \in \mathbb{R}^r$ in both dynamics and control (cost) objective function:

$$\Sigma(\theta) : \begin{array}{ll} \text{dynamics:} & \mathbf{x}_{t+1} = \mathbf{f}(\mathbf{x}_t, \mathbf{u}_t, \theta) \quad \text{with given } \mathbf{x}_0, \\ \text{control objective:} & J(\theta) = \sum_{t=0}^{T-1} c_t(\mathbf{x}_t, \mathbf{u}_t, \theta) + h(\mathbf{x}_T, \theta). \end{array} \quad (1)$$

Here, $\mathbf{x}_t \in \mathbb{R}^n$ is the system state; $\mathbf{u}_t \in \mathbb{R}^m$ is the control input; $\mathbf{f} : \mathbb{R}^n \times \mathbb{R}^m \times \mathbb{R}^r \mapsto \mathbb{R}^n$ is the dynamics model, which is assumed to be twice-differentiable; $t = 0, 1, \dots, T$ is the time step with T being the time horizon; and $J(\theta)$ is the control objective function with $c_t : \mathbb{R}^n \times \mathbb{R}^m \times \mathbb{R}^r \mapsto \mathbb{R}$ and $h : \mathbb{R}^n \times \mathbb{R}^r \mapsto \mathbb{R}$ denoting the stage/running and final costs, respectively, both of which are twice-differentiable. For a choice of θ , $\Sigma(\theta)$ will produce a trajectory of state-inputs:

$$\begin{aligned} \xi_\theta = \{\mathbf{x}_{0:T}^\theta, \mathbf{u}_{0:T-1}^\theta\} &\in \arg \min_{\{\mathbf{x}_{0:T}, \mathbf{u}_{0:T-1}\}} J(\theta) \\ \text{subject to} & \quad \mathbf{x}_{t+1} = \mathbf{f}(\mathbf{x}_t, \mathbf{u}_t, \theta) \text{ for all } t \text{ given } \mathbf{x}_0 \end{aligned} \quad (2)$$

that is, ξ_θ optimizes $J(\theta)$ subject to the dynamics constraint $\mathbf{f}(\theta)$. For many applications (we will show next), one evaluates the above ξ_θ using a scalar-valued differentiable loss $L(\xi_\theta, \theta)$. Then, the **problem of interest** is to tune the parameter θ , such that ξ_θ has the minimal loss:

$$\min_{\theta} L(\xi_\theta, \theta) \quad \text{subject to} \quad \xi_\theta \text{ is in (2)}. \quad (3)$$

Under the above base formulation, for a specific learning or control task, one only needs to accordingly change precise details of $\Sigma(\theta)$ and define a specific loss function $L(\xi_\theta, \theta)$, as we discuss below.

IRL/IOC Mode. Suppose that we are given optimal demonstrations $\xi^d = \{x_{0:T}^d, u_{0:T-1}^d\}$ of an expert optimal control system. We seek to learn the expert's dynamics and control objective function from ξ^d . To this end, we use $\Sigma(\theta)$ in (1) to represent the expert, and define the loss in (3) as

$$L(\xi_\theta, \theta) = l(\xi_\theta, \xi^d), \quad (4)$$

where l is a scalar function that penalizes the inconsistency of ξ_θ with ξ^d , e.g., $l(\xi_\theta, \xi^d) = \|\xi_\theta - \xi^d\|^2$. By solving (3) with (4), we can obtain a $\Sigma(\theta^*)$ whose trajectory is consistent with the observed demonstrations. It should be noted that even if the demonstrations ξ^d significantly deviate from the optimal ones, the above formulation still finds the 'best' control objective function (and dynamics) within the parameterized set $\Sigma(\theta)$ such that its reproduced ξ_θ in (2) has the *minimal distance* to ξ^d .

SysID Mode. Suppose that we are given data $\xi^o = \{x_{0:T}^o, u_{0:T-1}^o\}$ collected from, say, a physical system (here, unlike ξ^d , ξ^o is not necessarily optimal), and we wish to identify the system's dynamics. Here, $u_{0:T-1}^o$ are usually externally supplied to ensure the physical system is of persistent excitation [54]. In order for $\Sigma(\theta)$ in (1) to only represent dynamics (as we do not care about its internal control law), we set $J(\theta) = 0$. Then, ξ_θ in (2) accepts any $u_{0:T-1}^\theta = u_{0:T-1}^o$ as it always optimizes $J(\theta) = 0$. In other words, by setting $J(\theta) = 0$, $\Sigma(\theta)$ in (1) now only represent a class of dynamics models:

$\Sigma(\theta) :$	dynamics: $x_{t+1} = f(x_t, u_t, \theta)$ with x_0 and $u_{0:T-1}^\theta = u_{0:T-1}^o$.	(5)
--------------------	---	-----

Now, $\Sigma(\theta)$ produces $\xi_\theta = \{x_{0:T}^\theta, u_{0:T-1}^\theta\}$ subject to (5). To use (3) for identifying θ , we define

$$L(\xi_\theta, \theta) = l(\xi_\theta, \xi^o), \quad (6)$$

where l is to quantify the prediction error between ξ^o and ξ_θ under the same inputs $u_{0:T-1}$.

Control/Planning Mode. Consider a system with its dynamics learned in the above SysID. We want to obtain a *feedback controller* or *trajectory* such that the system achieves a performance of minimizing a given cost function. To that end, we specialize $\Sigma(\theta)$ in (1) as follows: first, set f as the learned dynamics and $J(\theta) = 0$; and second, through a *close-loop link*, we connect the input u_t and state x_t via a parameterized policy block $u_t = u(t, x_t, \theta)$ (reminder: unlike SysID Mode with u_t supplied externally, the inputs here are from a policy via a feedback loop). $\Sigma(\theta)$ now becomes

$\Sigma(\theta) :$	dynamics: $x_{t+1} = f(x_t, u_t)$ with x_0 , control policy: $u_t = u(t, x_t, \theta)$.	(7)
--------------------	---	-----

Now, $\Sigma(\theta)$ produces a trajectory $\xi_\theta = \{x_{0:T}^\theta, u_{0:T-1}^\theta\}$ subject to (7). We set the loss in (3) as

$$L(\xi_\theta, \theta) = \sum_{t=0}^{T-1} l(x_t^\theta, u_t^\theta) + l_f(x_T^\theta), \quad (8)$$

where l and l_f are the stage and final costs, respectively. Then, (3) is an optimal control or planning problem: if $u_t = u(t, x_t, \theta)$ (i.e., feedback policy explicitly depends on x_t), (3) is a *close-loop optimal control* problem; otherwise if $u_t = u(t, \theta)$ (e.g., polynomial parameterization), (3) is an *open-loop motion planning* problem. This mode can also be used as a component to solve (1) in IRL/IOC Mode.

4 An End-to-End Learning Framework

To solve the generic problem in (3), the idea of end-to-end learning [53] seeks to optimize the loss $L(\xi_\theta, \theta)$ directly with respect to the tunable parameter θ , by applying the gradient descent

$$\theta_{k+1} = \theta_k - \eta_k \frac{dL}{d\theta} \Big|_{\theta_k} \quad \text{with} \quad \frac{dL}{d\theta} \Big|_{\theta_k} = \frac{\partial L}{\partial \xi} \Big|_{\xi_{\theta_k}} \frac{\partial \xi_\theta}{\partial \theta} \Big|_{\theta_k} + \frac{\partial L}{\partial \theta} \Big|_{\theta_k}. \quad (9)$$

Here, $k = 0, 1, \dots$ is the iteration index; $\frac{dL}{d\theta} \Big|_{\theta_k}$ is the gradient of the loss with respect to θ evaluated at θ_k ; and η_k is the learning rate. From (9), we can draw a learning architecture in Fig. 2. Each update of θ consists of a *forward pass*, where at θ_k , the corresponding trajectory ξ_{θ_k} is solved from $\Sigma(\theta_k)$ and the loss is computed, and a *backward pass*, where $\frac{\partial L}{\partial \xi} \Big|_{\xi_{\theta_k}}$, $\frac{\partial \xi_\theta}{\partial \theta} \Big|_{\theta_k}$, and $\frac{\partial L}{\partial \theta} \Big|_{\theta_k}$ are computed.

In the forward pass, ξ_θ is obtained by solving an optimal control problem in $\Sigma(\theta)$ using any available OC methods, such as iLQR or Control/Planning Mode, (note that in SysID or Control/Planning modes, it is reduced to integrating difference equations (5) or (7)). In backward pass, $\frac{\partial L}{\partial \xi}$ and $\frac{\partial L}{\partial \theta}$ are easily obtained from the loss function $L(\xi_\theta, \theta)$. The main challenge, however, is to solve $\frac{\partial \xi_\theta}{\partial \theta}$, i.e., the derivative of a trajectory with respect to the parameters in the system. Next, we will analytically solve $\frac{\partial \xi_\theta}{\partial \theta}$ by proposing two techniques: *differential PMP* and *auxiliary control system*.

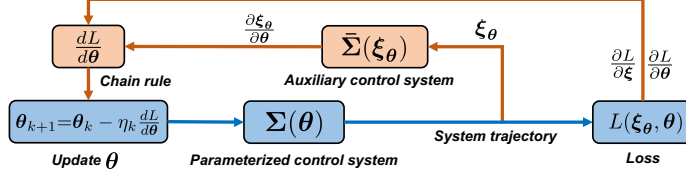


Figure 2: PDP end-to-end learning framework.

5 Key Contributions: Differential PMP & Auxiliary Control System

We first recall the discrete-time Pontryagin’s Maximum/Minimum Principle (PMP) [39] (a derivation of discrete-time PMP is given in Appendix C). For the optimal control system $\Sigma(\theta)$ in (1) with a fixed θ , PMP describes a set of optimality conditions which the trajectory $\xi_\theta = \{x_{0:T}^\theta, u_{0:T-1}^\theta\}$ in (2) must satisfy. To introduce these conditions, we first define the following *Hamiltonian*,

$$H_t = c_t(x_t, u_t; \theta) + f(x_t, u_t; \theta)' \lambda_{t+1}, \quad (10)$$

where $\lambda_t \in \mathbb{R}^n$ ($t = 1, 2, \dots, T$) is called the *costate variable*, which can be also thought of as the Lagrange multipliers for the dynamics constraints. According to PMP, there exists a sequence of costates $\lambda_{1:T}^\theta$, which together with the optimal trajectory $\xi_\theta = \{x_{0:T}^\theta, u_{0:T-1}^\theta\}$ satisfy

$$\text{dynamics equation:} \quad x_{t+1}^\theta = \frac{\partial H_t}{\partial \lambda_{t+1}^\theta} = f(x_t^\theta, u_t^\theta; \theta), \quad (11a)$$

$$\text{costate equation:} \quad \lambda_t^\theta = \frac{\partial H_t}{\partial x_t^\theta} = \frac{\partial c_t}{\partial x_t^\theta} + \frac{\partial f'}{\partial x_t^\theta} \lambda_{t+1}^\theta, \quad (11b)$$

$$\text{input equation:} \quad 0 = \frac{\partial H_t}{\partial u_t^\theta} = \frac{\partial c_t}{\partial u_t^\theta} + \frac{\partial f'}{\partial u_t^\theta} \lambda_{t+1}^\theta, \quad (11c)$$

$$\text{boundary conditions:} \quad \lambda_T^\theta = \frac{\partial h}{\partial x_T^\theta}, \quad x_0^\theta = x_0. \quad (11d)$$

For notation simplicity, $\frac{\partial g}{\partial x_t}$ means the derivative of function $g(x)$ with respect to x evaluated at x_t .

5.1 Differential PMP

To begin, recall that our goal (in Section 4) is to obtain $\frac{\partial \xi_\theta}{\partial \theta}$, that is,

$$\frac{\partial \xi_\theta}{\partial \theta} = \left\{ \frac{\partial x_{0:T}^\theta}{\partial \theta}, \frac{\partial u_{0:T-1}^\theta}{\partial \theta} \right\}. \quad (12)$$

To this end, we are motivated to differentiate the PMP conditions in (11) on both sides with respect to θ . This leads to the following *differential PMP*:

$$\text{differential dynamics equation:} \quad \frac{\partial x_{t+1}^\theta}{\partial \theta} = F_t \frac{\partial x_t^\theta}{\partial \theta} + G_t \frac{\partial u_t^\theta}{\partial \theta} + E_t, \quad (13a)$$

$$\text{differential costate equation:} \quad \frac{\partial \lambda_t^\theta}{\partial \theta} = H_t^{xx} \frac{\partial x_t^\theta}{\partial \theta} + H_t^{xu} \frac{\partial u_t^\theta}{\partial \theta} + F_t' \frac{\partial \lambda_{t+1}^\theta}{\partial \theta} + H_t^{xe}, \quad (13b)$$

$$\text{differential input equation:} \quad 0 = H_t^{ux} \frac{\partial x_t^\theta}{\partial \theta} + H_t^{uu} \frac{\partial u_t^\theta}{\partial \theta} + G_t' \frac{\partial \lambda_{t+1}^\theta}{\partial \theta} + H_t^{ue}, \quad (13c)$$

$$\text{differential boundary conditions:} \quad \frac{\partial \lambda_T^\theta}{\partial \theta} = H_T^{xx} \frac{\partial x_T^\theta}{\partial \theta} + H_T^{xe}, \quad \frac{\partial x_0^\theta}{\partial \theta} = \frac{\partial x_0}{\partial \theta} = 0. \quad (13d)$$

Here, to simplify notations and distinguish knowns and unknowns, the coefficient matrices in the above differential PMP (13) are defined as follows:

$$F_t = \frac{\partial f}{\partial x_t^\theta}, \quad G_t = \frac{\partial f}{\partial u_t^\theta}, \quad H_t^{xx} = \frac{\partial^2 H_t}{\partial x_t^\theta \partial x_t^\theta}, \quad H_t^{xe} = \frac{\partial^2 H_t}{\partial x_t^\theta \partial \theta}, \quad H_t^{xu} = \frac{\partial^2 H_t}{\partial x_t^\theta \partial u_t^\theta} = (H_t^{ux})', \quad (14a)$$

$$E_t = \frac{\partial f}{\partial \theta}, \quad H_t^{uu} = \frac{\partial^2 H_t}{\partial u_t^\theta \partial u_t^\theta}, \quad H_t^{ue} = \frac{\partial^2 H_t}{\partial u_t^\theta \partial \theta}, \quad H_T^{xx} = \frac{\partial^2 h}{\partial x_T^\theta \partial x_T^\theta}, \quad H_T^{xe} = \frac{\partial^2 h}{\partial x_T^\theta \partial \theta}, \quad (14b)$$

where we use $\frac{\partial^2 g}{\partial x_t \partial u_t}$ to denote the second-order derivative of a function $g(x, u)$ evaluated at (x_t, u_t) . Since the trajectory $\xi_\theta = \{x_{0:T}^\theta, u_{0:T-1}^\theta\}$ is obtained in the forward pass (recall Fig. 2), all matrices

in (14) are thus known (note that the computation of these matrices also requires $\lambda_{1:T}^\theta$, which can be obtained by iteratively solving (11b) and (11d) given ξ_θ). From the differential PMP in (13), we note that to obtain $\frac{\partial \xi_\theta}{\partial \theta}$ in (12), it is sufficient to compute the unknowns $\left\{ \frac{\partial x_{0:T}^\theta}{\partial \theta}, \frac{\partial x_{0:T-1}^\theta}{\partial \theta}, \frac{\partial \lambda_{1:T}^\theta}{\partial \theta} \right\}$ in (13). Next we will show that how these unknowns are elegantly solved by introducing a new system.

5.2 Auxiliary Control System

One important observation to the differential PMP in (13) is that it shares a similar structure to the original PMP in (11); so it can be viewed as a new set of PMP equations corresponding to an ‘oracle control optimal system’ whose the ‘optimal trajectory’ is exactly (12). This motivates us to ‘unearth’ this oracle optimal control system, because by doing so, (12) can be obtained from this oracle system by an OC solver. To this end, we first define the new ‘state’ and ‘control’ (matrix) variables:

$$X_t = \frac{\partial x_t}{\partial \theta} \in \mathbb{R}^{n \times r}, \quad U_t = \frac{\partial u_t}{\partial \theta} \in \mathbb{R}^{m \times r}, \quad (15)$$

respectively. Then, we ‘artificially’ define the following *auxiliary control system* $\bar{\Sigma}(\xi_\theta)$:

	dynamics: $X_{t+1} = F_t X_t + G_t U_t + E_t$ with $X_0 = \mathbf{0}$,	
$\bar{\Sigma}(\xi_\theta)$:	control objective:	$\bar{J} = \text{Tr} \sum_{t=0}^{T-1} \left(\frac{1}{2} \begin{bmatrix} X_t \\ U_t \end{bmatrix}' \begin{bmatrix} H_t^{xx} & H_t^{xu} \\ H_t^{ux} & H_t^{uu} \end{bmatrix} \begin{bmatrix} X_t \\ U_t \end{bmatrix} + \begin{bmatrix} H_t^{xe} \end{bmatrix}' \begin{bmatrix} X_t \\ U_t \end{bmatrix} \right) + \text{Tr} \left(\frac{1}{2} X_T' H_T^{xx} U_T + (H_T^{xe})' X_T \right). \quad (16)$

Here, $X_0 = \frac{\partial x_0}{\partial \theta} = \mathbf{0}$ because x_0 in (1) is given; \bar{J} is the defined control objective function which needs to be optimized in the auxiliary control system; and Tr denotes matrix trace. Before presenting the key results, we make some comments on the above auxiliary control system $\bar{\Sigma}(\xi_\theta)$. First, its state and control variables are both matrix variables defined in (15). Second, its dynamics is linear and control objective function \bar{J} is quadratic, for which the coefficient matrices are given in (14). Third, its dynamics and objective function are determined by the trajectory ξ_θ of the system $\Sigma(\theta)$ in forward pass, and this is why we denote it as $\bar{\Sigma}(\xi_\theta)$. Finally, we have the following important result.

Lemma 5.1. *Let $\{X_{0:T}^\theta, U_{0:T-1}^\theta\}$ be a stationary solution to the auxiliary control system $\bar{\Sigma}(\xi_\theta)$ in (16). Then, $\{X_{0:T}^\theta, U_{0:T-1}^\theta\}$ satisfies Pontryagin’s Maximum Principle of $\bar{\Sigma}(\xi_\theta)$, which is (13), and*

$$\{X_{0:T}^\theta, U_{0:T-1}^\theta\} = \left\{ \frac{\partial x_{0:T}^\theta}{\partial \theta}, \frac{\partial u_{0:T-1}^\theta}{\partial \theta} \right\} = \frac{\partial \xi_\theta}{\partial \theta}. \quad (17)$$

A proof of Lemma 5.1 is in Appendix A. Lemma 5.1 states two assertions. First, the PMP condition for the auxiliary control system $\bar{\Sigma}(\xi_\theta)$ is exactly the differential PMP in (13) for the original system $\Sigma(\theta)$; and second, importantly, the trajectory $\{X_{0:T}^\theta, U_{0:T-1}^\theta\}$ produced by the auxiliary control system $\bar{\Sigma}(\xi_\theta)$ is exactly the derivative of trajectory of the original system $\Sigma(\theta)$ with respect to the parameter θ . Based on Lemma 5.1, we can obtain $\frac{\partial \xi_\theta}{\partial \theta}$ from $\bar{\Sigma}(\xi_\theta)$ efficiently by the lemma below.

Lemma 5.2. *If H_t^{uu} in (16) is invertible for all $t = 0, 1, \dots, T-1$, define the following recursions*

$$P_t = Q_t + A_t'(I + P_{t+1}R_t)^{-1}P_{t+1}A_t, \quad (18a)$$

$$W_t = A_t'(I + P_{t+1}R_t)^{-1}(W_{t+1} + P_{t+1}M_t) + N_t, \quad (18b)$$

with $P_T = H_T^{xx}$ and $W_T = H_T^{xe}$. Here, I is identity matrix, $A_t = F_t - G_t(H_t^{uu})^{-1}H_t^{ux}$, $R_t = G_t(H_t^{uu})^{-1}G_t'$, $M_t = E_t - G_t(H_t^{uu})^{-1}H_t^{ue}$, $Q_t = H_t^{xx} - H_t^{xu}(H_t^{uu})^{-1}H_t^{ux}$, $N_t = H_t^{xe} - H_t^{xu}(H_t^{uu})^{-1}H_t^{ue}$ are all known given (14). Then, the stationary solution $\{X_{0:T}^\theta, U_{0:T-1}^\theta\}$ in (17) can be obtained by iteratively solving the following equations from $t = 0$ to $T-1$ with $X_0^\theta = X_0 = \mathbf{0}$:

$$U_t^\theta = -(H_t^{uu})^{-1} \left(H_t^{ux} X_t^\theta + H_t^{ue} + G_t'(I + P_{t+1}R_t)^{-1} (P_{t+1}A_t X_t^\theta + P_{t+1}M_t + W_{t+1}) \right), \quad (19a)$$

$$X_{t+1}^\theta = F_t X_t^\theta + G_t U_t^\theta + E_t. \quad (19b)$$

A proof of Lemma 5.2 is in Appendix B. Lemma 5.2 states that the trajectory of the above auxiliary control system $\bar{\Sigma}(\xi_\theta)$ can be obtained by two steps: first, iteratively solve (18) backward in time to

obtain matrices P_t and W_t (all other coefficient matrices are known given $\bar{\Sigma}(\xi_\theta)$); second, calculate $\{X_{0:T}^\theta, U_{0:T-1}^\theta\}$ by iteratively integrating a feedback-control system (19) forward in time. In fact, these two steps constitute the standard procedure to solve general finite-time LQR problems [55].

As a conclusion to the techniques developed in Section 5, in Algorithm 1 we summarize the procedure of computing $\frac{\partial \xi_\theta}{\partial \theta}$ via the introduced auxiliary control system. Algorithm 1 serves as a key component in the backward pass of the PDP learning framework, as shown in Fig. 2.

Algorithm 1: Solving $\frac{\partial \xi_\theta}{\partial \theta}$ using Auxiliary Control System (See details in Appendix D)

Input: The trajectory ξ_θ in (2) produced by the system $\Sigma(\theta)$ in (1) in the forward pass.

Compute the coefficient matrices (14) to obtain the auxiliary control system $\bar{\Sigma}(\xi_\theta)$ in (16);

Solve the auxiliary control system $\bar{\Sigma}(\xi_\theta)$ to obtain $\{X_{0:T}^\theta, U_{0:T-1}^\theta\}$ using Lemma 5.2;

Return: $\frac{\partial \xi_\theta}{\partial \theta} = \{X_{0:T}^\theta, U_{0:T-1}^\theta\}$

6 Applications to Different Learning Modes and Experiments

We investigate three learning modes of PDP, as described in Section 3. For each mode, we demonstrate its capability in four environments listed in Table 2, and a baseline and a state-of-the-art method are compared. Both PDP and environment codes are available at <https://github.com/wanxinjin>.

Table 2: Experimental environments (results for 6-DoF rocket landing is in Appendix I)

Systems	Dynamics parameter θ_{dyn}	Control objective parameter θ_{obj}
Cartpole	cart mass, pole mass and length	
Two-link robot arm	length and mass for each link	$c(x, u) = \ \theta'_{\text{obj}}(x - x_g)\ ^2 + \ u\ ^2$
6-DoF quadrotor maneuvering	mass, wing length, inertia matrix	$h(x, u) = \ \theta'_{\text{obj}}(x - x_g)\ ^2$
6-DoF rocket powered landing	mass, rocket length, inertia matrix	

We fix the unit weight to $\|u\|^2$, because estimating all weights will incur ambiguity [48]; x_g is the goal state.

IRL/IOC Mode. The parameterized $\Sigma(\theta)$ is in (1) and the loss in (4). In the forward pass of PDP, ξ_θ is solved from $\Sigma(\theta)$ by any OC solver. In the backward pass, $\frac{\partial \xi_\theta}{\partial \theta}$ is computed from the auxiliary control system $\bar{\Sigma}(\xi_\theta)$ in (16) using Algorithm 1. The full algorithm is in Appendix D.

Experiment: imitation learning. We use IRL/IOC Mode to solve imitation learning in environments in Table 2. The true dynamics is parameterized, and control objective is parameterized as a weighted distance to the goal, $\theta = \{\theta_{\text{dyn}}, \theta_{\text{obj}}\}$. Set imitation loss $L(\xi_\theta, \theta) = \|\xi^d - \xi_\theta\|^2$. Two other methods are compared: (i) neural policy cloning, and (ii) inverse KKT [52]. We set learning rate $\eta = 10^{-4}$ and run five trials given random initial θ_0 . The results in Fig. 3a-3c show that PDP significantly outperforms the policy cloning and inverse-KKT for a much lower training loss and faster convergence. In Fig. 3d, we apply the PDP to learn a neural control objective function for the robot arm using the same demonstration data in Fig. 3b, and we also compare with the GAIL [56]. Results in Fig. 3d show that the PDP successfully learns a neural objective function and the imitation loss of PDP is much lower than that of GAIL. It should note that because the demonstrations are not strictly realizable (optimal) under the parameterized neural objective function, the final loss for the PDP is small but not zero. This indicates that given sub-optimal demonstrations, PDP can still find the ‘best’ control objective function within the function set $J(\theta)$ such that its reproduced ξ_θ has the *minimal distance* to the demonstrations. Please refer to Appendix E.2 for more experiment details and additional validations.

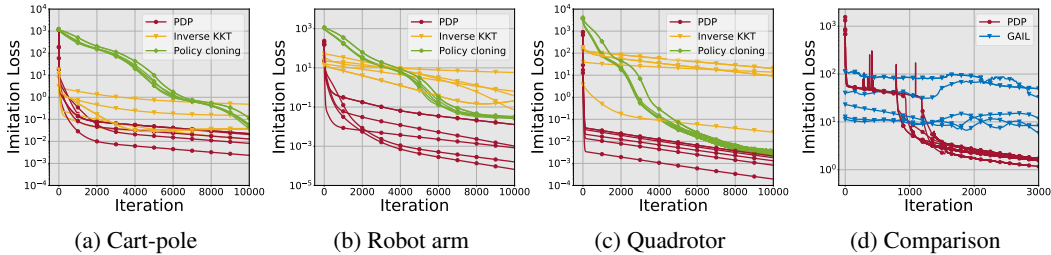


Figure 3: (a-c) imitation loss v.s. iteration, (d) PDP learns a neural objective function and comparison.

SysID Mode. In this mode, $\Sigma(\theta)$ is (5) and loss is (6). PDP is greatly simplified: in forward pass, ξ_θ is solved by integrating the difference equation (5). In the backward pass, $\bar{\Sigma}(\xi_\theta)$ is reduced to

$$\bar{\Sigma}(\xi_\theta) : \quad \text{dynamics: } X_{t+1}^\theta = F_t X_t^\theta + E_t \quad \text{with } X_0 = 0. \quad (20)$$

This is because $\Sigma(\theta)$ in (5) results from letting $J(\theta) = 0$, (13b-13d) and \bar{J} in (16) are then trivialized, and due to $u_{0:T-1}$ given, $U_t^\theta = 0$ in (13a). The algorithm is in Appendix D.

Experiment: system identification. We use the SysID Mode to identify the dynamics parameter θ_{dyn} for the systems in Table 2. Set the SysID loss $L(\xi_\theta, \theta) = \|\xi^\circ - \xi_\theta\|^2$. Two other methods are compared: (i) learning a neural network (NN) dynamics model, and (ii) DMDc [57]. For all methods, we set learning rate $\eta = 10^{-4}$, and run five trials with random θ_0 . The results are in Fig. 4. Fig. 4a-4c show an obvious advantage of PDP over the NN baseline and DMDc in terms of lower training loss and faster convergence speed. In Fig. 4d, we compare PDP and Adam [58] (here both with $\eta = 10^{-5}$) for training the same neural dynamics model for the robot arm. The results again show that PDP outperforms Adam for faster learning speed and lower training loss. Such advantages are due to that PDP has injected an inductive bias of optimal control into learning, making it more efficient for handling dynamical systems. More experiments and validations are in Appendix E.3.

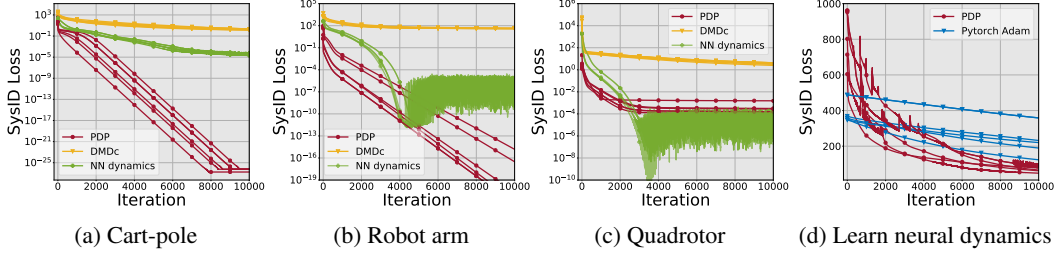


Figure 4: (a-c) SysID loss v.s. iteration, (d) PDP learns a neural dynamics model.

Control/Planning Mode. The parameterized system $\Sigma(\theta)$ is (7) and loss is (8). PDP for this mode is also simplified. In forward pass, ξ_θ is solved by integrating a (controlled) difference equation (7). In backward pass, \bar{J} in the auxiliary control system (16) is trivialized because we have considered $J(\theta) = 0$ in (7). Since the control is now given by $u_t = u(t, x_t, \theta)$, U_t^θ is obtained by differentiating the policy on both side with respect to θ , that is, $U_t^\theta = U_t^x X_t^\theta + U_t^e$ with $U_t^x = \frac{\partial u_t}{\partial x_t}$ and $U_t^e = \frac{\partial u_t}{\partial \theta}$. Thus,

$$\begin{aligned} \bar{\Sigma}(\xi_\theta) : \quad & \text{dynamics: } X_{t+1}^\theta = F_t X_t^\theta + G_t U_t^\theta \quad \text{with } X_0 = 0, \\ & \text{control policy: } U_t^\theta = U_t^x X_t^\theta + U_t^e. \end{aligned} \quad (21)$$

Integrating (21) from $t = 0$ to T leads to $\{X_{0:T}^\theta, U_{0:T-1}^\theta\} = \frac{\partial \xi_\theta}{\partial \theta}$. The algorithm is in Appendix D.

Experiment: control and planning. Based on identified dynamics, we learn policies of each system to optimize a control objective with given θ_{obj} . We set loss (8) as the control objective (below called control loss). To parameterize policy (7), we use a Lagrange polynomial of degree N (for planning) or neural network (for feedback control). iLQR [38] and guided policy search (GPS) [59] are compared. We set learning rate $\eta=10^{-4}$ or 10^{-6} and run five trials for each system. Fig. 5a-5b are learning neural network feedback policies for the cart-pole and robot arm, respectively. The results show that PDP outperforms GPS for having lower control loss. Fig. 5c is motion planning for quadrotor using a polynomial policy. It shows that PDP achieves a competitive performance with iLQR. Compared to iLQR, PDP minimizes over polynomial policies instead of input sequences, and thus has a higher final loss which depends on the expressiveness of the polynomial: e.g., the polynomial of degree $N=35$ has a lower loss than that of $N=5$. Since iLQR can be viewed as ‘1.5-order’ method (discussed in Section 2), it has faster converging speed than PDP which is only first-order, as shown in Fig. 5c. But iLQR is computationally extensive, PDP, instead, has a huge advantage of running time, as illustrated in Fig. 5d. Due to space constraint, we put detailed analysis between GPS and PDP in Appendix E.4.

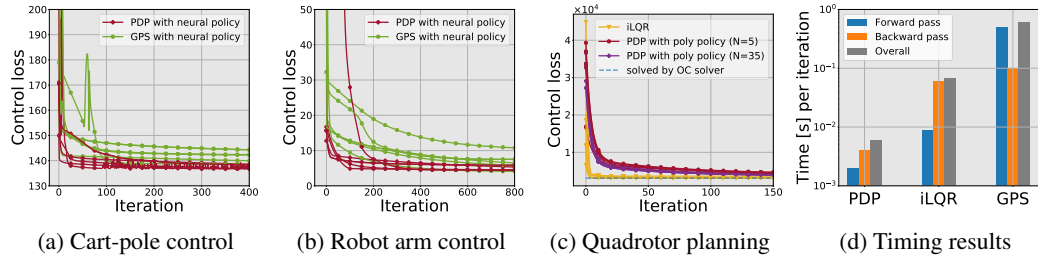


Figure 5: (a-c) control loss v.s. iteration, (d) comparison for running time per iteration.

7 Discussion

The related end-to-end learning frameworks. Two lines of recent work are related to PDP. One is the recent work [60–64] that seeks to replace a layer within a deep neural network by an *argmin layer*, in order to capture the information flow characterized by a solution of an optimization. Similar to PDP, these methods differentiate the argmin layer through KKT conditions. They mainly focus on static optimization problems, which can not directly be applied to dynamical systems. The second line is the recent RL development [65–68] that embeds an implicit planner within a policy. The idea is analogous to MPC, because using a predictive OC system (i.e., embedded planner) to generate controls leads to better adaption to unseen situations. The key problem in these methods is to learn a planner (i.e., OC system), which is similar to our formulation. [65, 66] learn a path-integral OC system [69], which is a special class of OC systems. [68] learns an OC system in a latent space. However, all these methods adopt the ‘unrolling’ strategy to facilitate differentiation. Specifically, they treat the forward pass of solving an OC problem as an ‘unrolled’ computational graph of multiple steps of applying gradient descent, because by this computational graph, automatic differentiation tool [70] can be immediately applied. The drawbacks of this ‘unrolling’ strategy are apparent: (i) they need to store all intermediate results over the entire computational graph, thus are memory-expensive; and (ii) the accuracy of gradient depends on the length of the ‘unrolled’ graph, thus facing trade-off between complexity and accuracy. To address these, [67] develops a differentiable MPC framework, where in forward pass, a LQR approximation of the OC system is obtained, and in backward pass, the gradient is solved by differentiating such LQR approximation. Although promising, this framework has one main weakness: differentiating LQR requires to solve a large linear equation, which involves the inverse of a matrix of size $(2n+m)T \times (2n+m)T$, thus can incur huge cost when handling systems of longer horizons T . Detailed descriptions for all these methods is in Appendix F.

Compared to [35, 65–68], the efficiency of PDP stems from the following novel aspects. First, in forward pass, without needing an unrolled computational graph, PDP only computes and stores the resulting trajectory of the OC system, ξ_θ , (does not care about how ξ_θ is solved). Second, without obtaining intermediate (LQR) approximations, PDP differentiates through PMP of the OC system to directly obtain the exact analytical gradient. Third, in the backward pass, unlike differentiable MPC which costs at least a complexity of $\mathcal{O}((m+2n)^2T^2)$ to differentiate a LQR approximation, PDP explicitly solves $\frac{\partial \xi_\theta}{\partial \theta}$ by an auxiliary control system, where thanks to the recursion structure, the memory and computation complexity of PDP is only $\mathcal{O}((m+2n)T)$. In Fig. 6, we have compared the running time of PDP with that of differentiable MPC. The results show PDP is 1000x faster than differentiable MPC. Due to space constraint, we put the detailed complexity analysis of PDP in Appendix G.

Convergence and limitation of PDP. Since all gradient quantities in PDP are analytical and exact, and the development of PDP does not involve any second-order derivative of functions or models, PDP essentially is a *first-order gradient-descent framework to solve non-convex bi-level optimization*. Therefore, in general, *PDP can only achieve local minima*. As explored by [71], if we pose further assumptions such as convexity and smoothness on all functions (dynamics, policy, loss, and control objective function), the global convergence of the bi-level programming could be established. But we do think these conditions are too restrictive for dynamical control systems. As a direction of future work, we will investigate the mild conditions for good convergence by taking advantage of control theory, e.g., Lyapunov theory. Due to space constraint, limitation of PDP is detailed in Appendix H.

8 Conclusions

This paper proposes a Pontryagin differentiable programming (PDP) methodology to establish an end-to-end learning framework for solving a range of learning and control tasks. The key contribution in PDP is that we incorporate the knowledge of optimal control theory as an inductive bias into the learning framework. Such combination enables PDP to achieve higher efficiency and capability than existing learning and control methods in solving many tasks including inverse reinforcement learning, system identification, and control/planning. We envision the proposed PDP could benefit to both learning and control fields for solving many high-dimensional continuous-space problems.

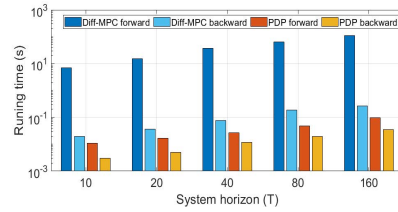


Figure 6: Runtime (per iteration) comparison between PDP and differentiable MPC for varying horizons of a pendulum system.

Broader Impact

This work is expected to have the impacts on both learning and control fields.

- To the learning field, this work connects some fundamental topics in machine learning to their counterparts in the control field, and unifies some concepts from reinforcement learning, backpropagation/deep learning, and control theory in one generic learning framework. The contribution of this framework is a deep integration of optimal control theory into end-to-end learning process, leading to an optimal-control-informed end-to-end learning framework that is flexible enough to solve a broad range of learning and control tasks and efficient enough to handle high-dimensional and continuous-space problems. In a broad perspective, we hope that this paper could motivate more future work that integrates the benefits of both control and learning to promote efficiency and explainability of artificial intelligence.
- To the control field, this work proposes a generic paradigm, which shows how a challenging control task can be converted into a learning formulation and solved using readily-available learning techniques, such as (deep) neural networks and backpropagation. For example, the proposed framework, equipped with (deep) neural networks, shows significant advantage for handling non-linear system identification and optimal control over state-of-the-art control methods. Since classic control theory typically requires knowledge of models, we expect that this work could pave a new way to extend classic control with data-driven techniques.

Since the formulation of this paper does not consider the boundness or constraints of a decision-making system, the real-world use of this work on physical systems might possibly raise safety issues during the training process; e.g., the state or input of the physical system at some time instance might exceeds the safety bounds that are physically required. One option to address this is to include these safety boundness as soft constraints added to the control objective or loss that is optimized. In future work, we will formally discuss PDP within a safety framework.

Acknowledgments and Disclosure of Funding

We acknowledge support for this research from Northrop Grumman Mission Systems' University Research Program.

References

- [1] Shixiang Gu, Timothy Lillicrap, Ilya Sutskever, and Sergey Levine. Continuous deep q-learning with model-based acceleration. In *International Conference on Machine Learning*, pages 2829–2838, 2016.
- [2] Nicolas Heess, Gregory Wayne, David Silver, Timothy Lillicrap, Tom Erez, and Yuval Tassa. Learning continuous control policies by stochastic value gradients. In *Advances in Neural Information Processing Systems*, pages 2944–2952, 2015.
- [3] Joshua L Proctor, Steven L Brunton, and J Nathan Kutz. Generalizing koopman theory to allow for inputs and control. *SIAM Journal on Applied Dynamical Systems*, 17(1):909–930, 2018.
- [4] Ian Abraham and Todd D Murphey. Active learning of dynamics for data-driven control using koopman operators. *IEEE Transactions on Robotics*, 35(5):1071–1083, 2019.
- [5] Rolf Johansson. *System modeling and identification*. Prentice Hall, 1993.
- [6] Bernard O Koopman. Hamiltonian systems and transformation in hilbert space. *Proceedings of the National Academy of Sciences of the United States of America*, 17(5):315, 1931.
- [7] Matthew O Williams, Ioannis G Kevrekidis, and Clarence W Rowley. A data-driven approximation of the koopman operator: Extending dynamic mode decomposition. *Journal of Nonlinear Science*, 25(6):1307–1346, 2015.
- [8] Masahiko Haruno, Daniel M Wolpert, and Mitsuo Kawato. Mosaic model for sensorimotor learning and control. *Neural computation*, 13(10):2201–2220, 2001.

- [9] Chelsea Finn, Ian Goodfellow, and Sergey Levine. Unsupervised learning for physical interaction through video prediction. In *Advances in Neural Information Processing Systems*, pages 64–72, 2016.
- [10] Manuel Watter, Jost Springenberg, Joschka Boedecker, and Martin Riedmiller. Embed to control: A locally linear latent dynamics model for control from raw images. In *Advances in Neural Information Processing Systems*, pages 2746–2754, 2015.
- [11] Katerina Fragkiadaki, Sergey Levine, Panna Felsen, and Jitendra Malik. Recurrent network models for human dynamics. In *IEEE International Conference on Computer Vision*, pages 4346–4354, 2015.
- [12] Marc Peter Deisenroth and Carl Edward Rasmussen. Pilco: A model-based and data-efficient approach to policy search. In *International Conference on Machine Learning*, pages 465–472, 2011.
- [13] Amy Zhang, Sainbayar Sukhbaatar, Adam Lerer, Arthur Szlam, and Rob Fergus. Composable planning with attributes. In *International Conference on Machine Learning*, pages 5842–5851, 2018.
- [14] Maziar Raissi, Paris Perdikaris, and George E Karniadakis. Physics-informed neural networks: A deep learning framework for solving forward and inverse problems involving nonlinear partial differential equations. *Journal of Computational Physics*, 378:686–707, 2019.
- [15] Steindor Saemundsson, Alexander Terenin, Katja Hofmann, and Marc Deisenroth. Variational integrator networks for physically structured embeddings. In *International Conference on Artificial Intelligence and Statistics*, pages 3078–3087, 2020.
- [16] Michael Lutter, Christian Ritter, and Jan Peters. Deep lagrangian networks: Using physics as model prior for deep learning. *arXiv preprint arXiv:1907.04490*, 2019.
- [17] Yaofeng Desmond Zhong, Biswadip Dey, and Amit Chakraborty. Symplectic ode-net: Learning hamiltonian dynamics with control. *arXiv preprint arXiv:1909.12077*, 2019.
- [18] Tian Qi Chen, Yulia Rubanova, Jesse Bettencourt, and David K Duvenaud. Neural ordinary differential equations. In *Advances in Neural Information Processing Systems*, pages 6571–6583, 2018.
- [19] Jiequn Han and Weinan E. Deep learning approximation for stochastic control problems. *Deep Reinforcement Learning Workshop, Advances in Neural Information Processing Systems*, 2016.
- [20] Qianxiao Li, Long Chen, Cheng Tai, and E Weinan. Maximum principle based algorithms for deep learning. *Journal of Machine Learning Research*, 18(1):5998–6026, 2017.
- [21] Qianxiao Li and Shuji Hao. An optimal control approach to deep learning and applications to discrete-weight neural networks. *arXiv preprint arXiv:1803.01299*, 2018.
- [22] Weinan E, Jiequn Han, and Qianxiao Li. A mean-field optimal control formulation of deep learning. *Research in the Mathematical Sciences*, 6(1), 2019.
- [23] Dinghuai Zhang, Tianyuan Zhang, Yiping Lu, Zhanxing Zhu, and Bin Dong. You only propagate once: Painless adversarial training using maximal principle. *arXiv preprint arXiv:1905.00877*, 2019.
- [24] Martin Benning, Elena Celledoni, Matthias J Ehrhardt, Brynjulf Owren, and Carola-Bibiane Schönlieb. Deep learning as optimal control problems: models and numerical methods. *arXiv preprint arXiv:1904.05657*, 2019.
- [25] Hailiang Liu and Peter Markowich. Selection dynamics for deep neural networks. *arXiv preprint arXiv:1905.09076*, 2019.
- [26] Junhyuk Oh, Valliappa Chockalingam, Satinder Singh, and Honglak Lee. Control of memory, active perception, and action in minecraft. *arXiv preprint arXiv:1605.09128*, 2016.

- [27] Volodymyr Mnih, Koray Kavukcuoglu, David Silver, Alex Graves, Ioannis Antonoglou, Daan Wierstra, and Martin Riedmiller. Playing atari with deep reinforcement learning. *arXiv preprint arXiv:1312.5602*, 2013.
- [28] Volodymyr Mnih, Koray Kavukcuoglu, David Silver, Andrei A Rusu, Joel Veness, Marc G Bellemare, Alex Graves, Martin Riedmiller, Andreas K Fidjeland, Georg Ostrovski, et al. Human-level control through deep reinforcement learning. *Nature*, 518(7540):529, 2015.
- [29] Jeff G Schneider. Exploiting model uncertainty estimates for safe dynamic control learning. In *Advances in Neural Information Processing Systems*, pages 1047–1053, 1997.
- [30] Pieter Abbeel, Morgan Quigley, and Andrew Y Ng. Using inaccurate models in reinforcement learning. In *International Conference on Machine Learning*, pages 1–8, 2006.
- [31] Sergey Levine and Pieter Abbeel. Learning neural network policies with guided policy search under unknown dynamics. In *Advances in Neural Information Processing Systems*, pages 1071–1079, 2014.
- [32] Richard S Sutton. Dyna, an integrated architecture for learning, planning, and reacting. *ACM Sigart Bulletin*, 2(4):160–163, 1991.
- [33] Eric Tzeng, Coline Devin, Judy Hoffman, Chelsea Finn, Pieter Abbeel, Sergey Levine, Kate Saenko, and Trevor Darrell. Adapting deep visuomotor representations with weak pairwise constraints. In *Algorithmic Foundations of Robotics XII*, pages 688–703. Springer, 2020.
- [34] Michael Janner, Justin Fu, Marvin Zhang, and Sergey Levine. When to trust your model: Model-based policy optimization. In *Advances in Neural Information Processing Systems*, pages 12519–12530, 2019.
- [35] Aviv Tamar, Yi Wu, Garrett Thomas, Sergey Levine, and Pieter Abbeel. Value iteration networks. In *Advances in Neural Information Processing Systems*, pages 2154–2162, 2016.
- [36] Jiongmin Yong and Xun Yu Zhou. *Stochastic controls: Hamiltonian systems and HJB equations*, volume 43. Springer Science & Business Media, 1999.
- [37] David H Jacobson and David Q Mayne. Differential dynamic programming. 1970.
- [38] Weiwei Li and Emanuel Todorov. Iterative linear quadratic regulator design for nonlinear biological movement systems. In *International Conference on Informatics in Control, Automation and Robotics*, pages 222–229, 2004.
- [39] Lev Semenovich Pontryagin, V. G. Boltyanskiy, R. V. Gamkrelidze, and E. F. Mishchenko. *The Mathematical Theory of Optimal Processes*. John Wiley & Sons, Inc., 1962.
- [40] Hans Georg Bock and Karl-Josef Plitt. A multiple shooting algorithm for direct solution of optimal control problems. *IFAC Proceedings Volumes*, 17(2):1603–1608, 1984.
- [41] Michael A Patterson and Anil V Rao. Gpops-ii: A matlab software for solving multiple-phase optimal control problems using hp-adaptive gaussian quadrature collocation methods and sparse nonlinear programming. *ACM Transactions on Mathematical Software*, 41(1):1, 2014.
- [42] Eduardo F Camacho and Carlos Bordons Alba. *Model predictive control*. Springer Science & Business Media, 2013.
- [43] S Joe Qin and Thomas A Badgwell. An overview of nonlinear model predictive control applications. In *Nonlinear model predictive control*, pages 369–392. Springer, 2000.
- [44] Yang Wang and Stephen Boyd. Fast model predictive control using online optimization. *IEEE Transactions on control systems technology*, 18(2):267–278, 2009.
- [45] Pieter Abbeel and Andrew Y Ng. Apprenticeship learning via inverse reinforcement learning. In *International Conference on Machine Learning*, pages 1–8, 2004.

- [46] Brian D Ziebart, Andrew Maas, J Andrew Bagnell, and Anind K Dey. Maximum entropy inverse reinforcement learning. In *AAAI Conference on Artificial Intelligence*, pages 1433–1438, 2008.
- [47] Nathan D Ratliff, J Andrew Bagnell, and Martin A Zinkevich. Maximum margin planning. In *International Conference on Machine Learning*, pages 729–736, 2006.
- [48] Arezou Keshavarz, Yang Wang, and Stephen Boyd. Imputing a convex objective function. In *IEEE International Symposium on Intelligent Control*, pages 613–619, 2011.
- [49] Katja Mombaur, Anh Truong, and Jean-Paul Laumond. From human to humanoid locomotion—an inverse optimal control approach. *Autonomous Robots*, 28(3):369–383, 2010.
- [50] Wanxin Jin, Dana Kulić, Shaoshuai Mou, and Sandra Hirche. Inverse optimal control from incomplete trajectory observations. *arXiv preprint arXiv:1803.07696*, 2018.
- [51] Wanxin Jin, Dana Kulić, Jonathan Feng-Shun Lin, Shaoshuai Mou, and Sandra Hirche. Inverse optimal control for multiphase cost functions. *IEEE Transactions on Robotics*, 35(6):1387–1398, 2019.
- [52] Peter Englert, Ngo Anh Vien, and Marc Toussaint. Inverse kkt: Learning cost functions of manipulation tasks from demonstrations. *The International Journal of Robotics Research*, 36(13-14):1474–1488, 2017.
- [53] Urs Muller, Jan Ben, Eric Cosatto, Beat Flepp, and Yann L Cun. Off-road obstacle avoidance through end-to-end learning. In *Advances in Neural Information Processing Systems*, pages 739–746, 2006.
- [54] Michael Green and John B Moore. Persistence of excitation in linear systems. *Systems & control letters*, 7(5):351–360, 1986.
- [55] Huibert Kwakernaak and Raphael Sivan. *Linear optimal control systems*, volume 1. New York: Wiley-Interscience, 1972.
- [56] Jonathan Ho and Stefano Ermon. Generative adversarial imitation learning. *arXiv preprint arXiv:1606.03476*, 2016.
- [57] Joshua L Proctor, Steven L Brunton, and J Nathan Kutz. Dynamic mode decomposition with control. *SIAM Journal on Applied Dynamical Systems*, 15(1):142–161, 2016.
- [58] Diederik P Kingma and Jimmy Ba. Adam: A method for stochastic optimization. *International Conference on Learning Representations*, 2015.
- [59] Sergey Levine and Vladlen Koltun. Guided policy search. In *International Conference on Machine Learning*, pages 1–9, 2013.
- [60] Brandon Amos and J Zico Kolter. Optnet: Differentiable optimization as a layer in neural networks. *International Conference on Machine Learning*, 2017.
- [61] Po-Wei Wang, Priya L Donti, Bryan Wilder, and Zico Kolter. Satnet: Bridging deep learning and logical reasoning using a differentiable satisfiability solver. *International Conference on Machine Learning*, 2019.
- [62] Bryan Wilder, Bistra Dilkina, and Milind Tambe. Melding the data-decisions pipeline: Decision-focused learning for combinatorial optimization. In *AAAI Conference on Artificial Intelligence*, volume 33, pages 1658–1665, 2019.
- [63] Filipe de Avila Belbute-Peres, Kevin Smith, Kelsey Allen, Josh Tenenbaum, and J Zico Kolter. End-to-end differentiable physics for learning and control. In *Advances in Neural Information Processing Systems*, pages 7178–7189, 2018.
- [64] Priya Donti, Brandon Amos, and J Zico Kolter. Task-based end-to-end model learning in stochastic optimization. In *Advances in Neural Information Processing Systems*, pages 5484–5494, 2017.

- [65] Masashi Okada, Luca Rigazio, and Takenobu Aoshima. Path integral networks: End-to-end differentiable optimal control. *arXiv preprint arXiv:1706.09597*, 2017.
- [66] Marcus Pereira, David D Fan, Gabriel Nakajima An, and Evangelos Theodorou. Mpc-inspired neural network policies for sequential decision making. *arXiv preprint arXiv:1802.05803*, 2018.
- [67] Brandon Amos, Ivan Jimenez, Jacob Sacks, Byron Boots, and J Zico Kolter. Differentiable mpc for end-to-end planning and control. In *Advances in Neural Information Processing Systems*, pages 8289–8300, 2018.
- [68] Aravind Srinivas, Allan Jabri, Pieter Abbeel, Sergey Levine, and Chelsea Finn. Universal planning networks. *arXiv preprint arXiv:1804.00645*, 2018.
- [69] Hilbert J Kappen. Path integrals and symmetry breaking for optimal control theory. *Journal of Statistical Mechanics: Theory and Experiment*, 2005.
- [70] Martín Abadi, Ashish Agarwal, Paul Barham, Eugene Brevdo, Zhifeng Chen, Craig Citro, Greg S Corrado, Andy Davis, Jeffrey Dean, Matthieu Devin, et al. Tensorflow: Large-scale machine learning on heterogeneous distributed systems. *arXiv preprint arXiv:1603.04467*, 2016.
- [71] Saeed Ghadimi and Mengdi Wang. Approximation methods for bilevel programming. *arXiv preprint arXiv:1802.02246*, 2018.
- [72] Michael Athans. The matrix minimum principle. *Information and Control*, 11(5-6):592–606, 1967.
- [73] Mordecai Avriel. *Nonlinear programming: analysis and methods*. Courier Corporation, 2003.
- [74] Daniel Liberzon. *Calculus of variations and optimal control theory: a concise introduction*. Princeton University Press, 2011.
- [75] Jack B Kuipers. *Quaternions and rotation sequences*, volume 66. Princeton University Press, 1999.
- [76] Taeyoung Lee, Melvin Leok, and N Harris McClamroch. Geometric tracking control of a quadrotor uav on $se(3)$. In *IEEE Conference on Decision and Control*, pages 5420–5425, 2010.
- [77] Mark W Spong and Mathukumalli Vidyasagar. *Robot dynamics and control*. John Wiley & Sons, 2008.
- [78] Mariusz Bojarski, Davide Del Testa, Daniel Dworakowski, Bernhard Firner, Beat Flepp, Praseen Goyal, Lawrence D Jackel, Mathew Monfort, Urs Muller, Jiakai Zhang, et al. End to end learning for self-driving cars. *arXiv preprint arXiv:1604.07316*, 2016.
- [79] Joel A E Andersson, Joris Gillis, Greg Horn, James B Rawlings, and Moritz Diehl. CasADi – A software framework for nonlinear optimization and optimal control. *Mathematical Programming Computation*, 11(1):1–36, 2019.
- [80] Milton Abramowitz and Irene A Stegun. *Handbook of mathematical functions with formulas, graphs, and mathematical tables*, volume 55. U.S. Government Printing Office, 1948.
- [81] Gamal Elnagar, Mohammad A Kazemi, and Mohsen Razzaghi. The pseudospectral legendre method for discretizing optimal control problems. *IEEE Transactions on Automatic Control*, 40(10):1793–1796, 1995.
- [82] Aviv Tamar, Garrett Thomas, Tianhao Zhang, Sergey Levine, and Pieter Abbeel. Learning from the hindsight plan—episodic mpc improvement. In *IEEE International Conference on Robotics and Automation*, pages 336–343, 2017.
- [83] Peng Xu, Fred Roosta, and Michael W Mahoney. Second-order optimization for non-convex machine learning: An empirical study. In *SIAM International Conference on Data Mining*, pages 199–207, 2020.
- [84] Michael Szmuk and Behcet Acikmese. Successive convexification for 6-dof mars rocket powered landing with free-final-time. In *AIAA Guidance, Navigation, and Control Conference*, page 0617, 2018.

A Proof of Lemma 5.1

To prove Lemma 5.1, we just need to show that the Pontryagin's Maximum Principle for the auxiliary control system $\bar{\Sigma}(\xi_\theta)$ in (16) is exactly the differential PMP in (13). To this end, we define the following Hamiltonian for the auxiliary control system $\bar{\Sigma}(\xi_\theta)$:

$$\bar{H}_t = \text{Tr} \left(\frac{1}{2} \begin{bmatrix} X_t \\ U_t \end{bmatrix}' \begin{bmatrix} H_t^{xx} & H_t^{xu} \\ H_t^{ux} & H_t^{uu} \end{bmatrix} \begin{bmatrix} X_t \\ U_t \end{bmatrix} + \begin{bmatrix} H_t^{xe} \\ H_t^{ue} \end{bmatrix}' \begin{bmatrix} X_t \\ U_t \end{bmatrix} \right) + \text{Tr} (\Lambda_{t+1}' (F_t X_t + G_t U_t + E_t)), \quad (\text{S.1})$$

with $t = 0, 1, \dots, T-1$. Here $\Lambda_{t+1} \in \mathbb{R}^{n \times r}$ denotes the costate (matrix) variables for the auxiliary control system. Based on Section 3 in [72], there exists a sequence of costates $\Lambda_{1:T}^\theta$, which together the stationary solution $\{X_{0:T}^\theta, U_{0:T-1}^\theta\}$ to the auxiliary control system must satisfy the following the matrix version of PMP (we here follow the notation style used in (11)).

The dynamics equation:

$$\begin{aligned} \frac{\partial \bar{H}_t}{\partial \Lambda_{t+1}^\theta} &= \frac{\partial \text{Tr} (\Lambda_{t+1}' (F_t X_t + G_t U_t + E_t))}{\partial \Lambda_{t+1}} \bigg|_{\substack{\Lambda_{t+1} = \Lambda_{t+1}^\theta \\ X_t = X_t^\theta \\ U_t = U_t^\theta}} \\ &= F_t X_t^\theta + G_t U_t^\theta + E_t = \mathbf{0}. \end{aligned} \quad (\text{S.2a})$$

The costate equation:

$$\begin{aligned} \frac{\partial \bar{H}_t}{\partial X_t^\theta} &= \frac{\partial \text{Tr} (\frac{1}{2} X_t' H_t^{xx} X_t) + \partial \text{Tr} (U_t' H_t^{ux} X_t) + \partial \text{Tr} (H_t^{ex} X_t) + \partial \text{Tr} (\Lambda_{t+1}' F_t X_t)}{\partial X_t} \bigg|_{\substack{\Lambda_{t+1} = \Lambda_{t+1}^\theta \\ X_t = X_t^\theta \\ U_t = U_t^\theta}} \\ &= H_t^{xx} X_t^\theta + H_t^{xu} U_t^\theta + H_t^{xe} + F_t' \Lambda_{t+1}^\theta = \Lambda_t^\theta. \end{aligned} \quad (\text{S.2b})$$

Input equation:

$$\begin{aligned} \frac{\partial \bar{H}_t}{\partial U_t^\theta} &= \frac{\partial \text{Tr} (\frac{1}{2} U_t' H_t^{uu} U_t) + \partial \text{Tr} (U_t' H_t^{ux} X_t) + \partial \text{Tr} (H_t^{eu} U_t) + \partial \text{Tr} (\Lambda_{t+1}' G_t U_t)}{\partial U_t} \bigg|_{\substack{\Lambda_{t+1} = \Lambda_{t+1}^\theta \\ X_t = X_t^\theta \\ U_t = U_t^\theta}} \\ &= H_t^{uu} U_t^\theta + H_t^{ux} X_t^\theta + H_t^{ue} + G_t' \Lambda_{t+1}^\theta = \mathbf{0}. \end{aligned} \quad (\text{S.2c})$$

And boundary conditions:

$$\Lambda_T^\theta = \frac{\partial \text{Tr} (\frac{1}{2} X_T' H_T^{xx} X_T) + \partial \text{Tr} ((H_T^{xe})' X_T)}{\partial X_T} \bigg|_{X_T = X_T^\theta} = H_T^{xx} X_T^\theta + H_T^{xe}, \quad (\text{S.2d})$$

and $X_0^\theta = \mathbf{0}$. Note that in the above derivations, we used the following matrix calculus [72]:

$$\frac{\partial \text{Tr}(AB)}{\partial A} = B', \quad \frac{\partial f(A)}{\partial A'} = \left[\frac{\partial f(A)}{\partial A} \right]', \quad \frac{\partial \text{Tr}(X' H X)}{\partial X} = H X + H' X, \quad (\text{S.3})$$

and the following matrix trace properties:

$$\text{Tr}(A) = \text{Tr}(A'), \quad \text{Tr}(ABC) = \text{Tr}(BCA) = \text{Tr}(CAB), \quad \text{Tr}(A+B) = \text{Tr}(A) + \text{Tr}(B). \quad (\text{S.4})$$

Since the above obtained PMP equations (S.2) are the same with the differential PMP in (13), we thus can conclude that the Pontryagin's Maximum Principle of the auxiliary control system $\bar{\Sigma}(\xi_\theta)$ in (16) is exactly the differential PMP equations (13), and thus (17) holds. This completes the proof. \square

B Proof of Lemma 5.2

Based on Lemma 5.1 and its proof, we known that the PMP of the auxiliary control system, (S.2), is exactly the differential PMP equations (13). Thus below, we only look at the differential PMP equations in (S.2). From (S.2c), we solve for U_t^θ (if H_t^{uu} invertible):

$$U_t^\theta = -(H_t^{uu})^{-1} (H_t^{ux} X_t^\theta + G_t' \Lambda_{t+1}^\theta + H_t^{ue}). \quad (\text{S.5})$$

By substituting (S.5) into (S.2a) and (S.2b), respectively, and considering the definitions of matrices A_t, R_t, M_t, Q_t and N_t in (18), we have

$$X_{t+1}^\theta = A_t X_t^\theta - R_t \Lambda_{t+1}^\theta + M_t, \quad (\text{S.6})$$

$$\Lambda_t^\theta = Q_t X_t^\theta + A_t' \Lambda_{t+1}^\theta + N_t, \quad (\text{S.7})$$

for $t = 0, 1, \dots, T-1$, and also the boundary condition in (S.2d)

$$\Lambda_T^\theta = H_T^{xx} X_T^\theta + H_T^{xe},$$

for $t = T$. Next, we prove that there exist matrices P_t and W_t such that

$$\Lambda_t^\theta = P_t X_t^\theta + W_t. \quad (\text{S.8})$$

Proof by induction: (S.2d) shows that (S.8) holds for $t = T$ if $P_T = H_T^{xx}$ and $W_T = H_T^{xe}$. Assume (S.8) holds for $t+1$, then by manipulating (S.6) and (S.7), we have

$$\Lambda_t^\theta = \underbrace{(Q_t + A_t'(I + P_{t+1}R_t)^{-1}P_{t+1}A_t)}_{P_t} X_t^\theta + \underbrace{A_t'(I + P_{t+1}R_t)^{-1}(W_{t+1} + P_{t+1}M_t) + N_t}_{W_t}, \quad (\text{S.9})$$

which indicates (S.8) holds for t , if P_t and W_t satisfy (18a) and (18b), respectively. Substituting (S.8) to (S.7) and also considering (S.5) will lead to (19a). (19b) directly results from (S.2a). We complete the proof. \square

C Proof of the Discrete-Time Pontryagin's Maximum Principle

We here provide an easy-approach derivation of the discrete-time PMP based on Karush-Kuhn-Tucker (KKT) conditions in non-linear optimization [73]. The original derivation for continuous optimal control systems uses the calculus of variation theory, which can be found in [39] and [74].

We view the optimal control system (1) with a fixed θ as a constrained optimization problem, where the objective function is given by $J(\theta)$ and the constraints given by dynamics $f(\theta)$. Define the following Lagrangian for this constrained optimization problem:

$$\begin{aligned} L &= J(\theta) + \sum_{t=0}^{T-1} \lambda'_{t+1} (f(x_t, u_t, \theta) - x_{t+1}) \\ &= \sum_{t=0}^{T-1} \left(c_t(x_t, u_t, \theta) + \lambda'_{t+1} (f(x_t, u_t, \theta) - x_{t+1}) \right) + h(x_T, \theta) \\ &= \sum_{t=0}^{T-1} \left(H_t - \lambda'_{t+1} x_{t+1} \right) + h(x_T, \theta), \end{aligned} \quad (\text{S.10})$$

where λ_t is the Lagrange multiplier for the dynamics constraint for $t = 1, 2, \dots, T$, and the third line in (S.10) is due to the definition of Hamiltonian in (10). According to the KKT conditions, for the optimal solution $\xi_\theta = \{x_{0:T}^\theta, u_{0:T-1}^\theta\}$, there must exist the multipliers $\lambda_{1:T}^\theta$ (in optimal control they are called costates) such that the following first-order conditions are satisfied:

$$\frac{\partial L}{\partial \lambda_{1:T}^\theta} = \mathbf{0}, \quad \frac{\partial L}{\partial x_{0:T}^\theta} = \mathbf{0}, \quad \frac{\partial L}{\partial u_{0:T-1}^\theta} = \mathbf{0}. \quad (\text{S.11})$$

By extending the above three conditions in (S.11) at each λ_t, x_t and u_t , respectively, and particularly taking care of x_T , we will obtain

$$\mathbf{0} = f(x_t^\theta, u_t^\theta; \theta) - x_{t+1}^\theta, \quad (\text{S.12a})$$

$$\mathbf{0} = \frac{\partial H_t}{\partial x_t^\theta} - \lambda_t^\theta = \frac{\partial c_t}{\partial x_t^\theta} + \frac{\partial f'}{\partial x_t^\theta} \lambda_{t+1}^\theta - \lambda_t^\theta, \quad (\text{S.12b})$$

$$\mathbf{0} = \frac{\partial H_t}{\partial u_t^\theta} = \frac{\partial c_t}{\partial u_t^\theta} + \frac{\partial f'}{\partial u_t^\theta} \lambda_{t+1}^\theta, \quad (\text{S.12c})$$

$$\mathbf{0} = \frac{\partial h}{\partial x_T^\theta} - \lambda_T^\theta, \quad (\text{S.12d})$$

respectively, which are exactly the PMP equations in (11). This completes the proof. \square

D Algorithms Details for Different Learning Modes

Algorithm 2: Solving $\frac{\partial \xi_\theta}{\partial \theta}$ using Auxiliary Control System

Input: The trajectory ξ_θ generated by the system $\Sigma(\theta)$

Compute the coefficient matrices (14) to obtain the auxiliary control system $\bar{\Sigma}(\xi_\theta)$ in (16);

def Auxiliary_Control_System_Solver ($\bar{\Sigma}(\xi_\theta)$): \triangleright implementation of Lemma 5.2

Set $P_T = H_T^{xx}$ and $W_T = H_T^{xe}$;

for $t \leftarrow T$ **to** 0 **by** -1 **do**

Update P_t and W_t using equations (18);

\triangleright backward in time

end

Set $X_0^\theta = 0$;

for $t \leftarrow 0$ **to** T **by** 1 **do**

Update X_t^θ and U_t^θ using equations (19);

\triangleright forward in time

end

Return: $\{X_{0:T}^\theta, U_{0:T-1}^\theta\}$

Return: $\frac{\partial \xi_\theta}{\partial \theta} = \{X_{0:T}^\theta, U_{0:T-1}^\theta\}$

Algorithm 3: PDP Algorithm for IRL/IOC Mode

Data : Expert demonstrations $\{\xi^d\}$

Parameterization: The parameterized optimal control system $\Sigma(\theta)$ in (1)

Loss: $L(\xi_\theta, \theta)$ in (4)

Initialization : θ_0 , learning rate $\{\eta_k\}_{k=0,1,\dots}$

for $k = 0, 1, 2, \dots$ **do**

Solve ξ_{θ_k} from the current optimal control system $\Sigma(\theta_k)$; \triangleright using any OC solver

Obtain $\frac{\partial \xi_\theta}{\partial \theta} \big|_{\theta_k}$ using Algorithm 2 given ξ_{θ_k} ; \triangleright using Algorithm 2

Obtain $\frac{\partial L}{\partial \xi} \big|_{\xi_{\theta_k}}$ from the given loss function $L(\xi_\theta, \theta)$;

Apply the chain rule (9) to obtain $\frac{dL}{d\theta} \big|_{\theta_k}$;

Update $\theta_{k+1} \leftarrow \theta_k - \eta_k \frac{dL}{d\theta} \big|_{\theta_k}$;

end

Algorithm 4: PDP Algorithm for SysID Mode

Data: Input-state data $\{\xi^o\}$

Parameterization: The parameterized dynamics model $\Sigma(\theta)$ in (5)

Loss: $L(\xi_\theta, \theta)$ in (6)

Initialization: θ_0 , learning rate $\{\eta_k\}_{k=0,1,\dots}$

for $k = 0, 1, 2, \dots$ **do**

Obtain ξ_{θ_k} by iteratively integrating $\Sigma(\theta_k)$ in (5) for $t = 0, \dots, T - 1$;

Compute the coefficient matrices (14) to obtain the auxiliary control system $\bar{\Sigma}(\xi_\theta)$ in (20);

Obtain $\frac{\partial \xi_\theta}{\partial \theta} \big|_{\theta_k}$ by iteratively integrating $\bar{\Sigma}(\xi_{\theta_k})$ in (20) for $t = 0, \dots, T - 1$;

Obtain $\frac{\partial L}{\partial \xi} \big|_{\xi_{\theta_k}}$ from the given loss function in (6);

Apply the chain rule (9) to obtain $\frac{dL}{d\theta} \big|_{\theta_k}$;

Update $\theta_{k+1} \leftarrow \theta_k - \eta_k \frac{dL}{d\theta} \big|_{\theta_k}$;

end

Algorithm 5: PDP Algorithm for Control/Planning Mode

Parameterization: The parameterized-policy system $\Sigma(\theta)$ in (7)

Loss: $L(\xi_\theta, \theta)$ in (8)

Initialization: θ_0 , learning rate $\{\eta_k\}_{k=0,1,\dots}$

for $k = 0, 1, 2, \dots$ **do**

 Obtain ξ_{θ_k} by iteratively integrating $\Sigma(\theta_k)$ in (7) for $t = 0, \dots, T - 1$;

 Compute the coefficient matrices (14) to obtain the auxiliary control system $\bar{\Sigma}(\xi_\theta)$ in (21);

 Obtain $\frac{\partial \xi_\theta}{\partial \theta} \big|_{\theta_k}$ by iteratively integrating $\bar{\Sigma}(\xi_{\theta_k})$ in (21) for $t = 0, \dots, T - 1$;

 Obtain $\frac{\partial L}{\partial \xi} \big|_{\xi_{\theta_k}}$ from the given loss function $L(\xi_\theta, \theta)$ in (8);

 Apply the chain rule (9) to obtain $\frac{dL}{d\theta} \big|_{\theta_k}$;

 Update $\theta_{k+1} \leftarrow \theta_k - \eta_k \frac{dL}{d\theta} \big|_{\theta_k}$;

end

Additional comments: combining different learning modes. In addition to using different learning modes to solve different types of problems, one can combine different modes in a single learning task. For example, when solving model-based reinforcement learning, one can call SysID Mode to first learn a dynamics model, then use the learned dynamics in Control/Planning Mode to obtain an optimal policy. In problems such as imitation learning, one can first learn a dynamics model using SysID Mode, then use the learned dynamics as the initial guess in IRL/IOC Mode. In forward pass of IOC/IRL Mode, one can call Control/Planning Mode to solve the OC system. For control and planning problems, the loss required in Control/Planning Mode can be learned using IOC/IRL Mode. In MPC-based learning and control [67], one can use the general formulation in (3) to learn a MPC controller, and then execute the MPC controller by calling Control/Planning Mode.

E Experiment Details

We have released the PDP source codes and different simulation environments/systems in this paper as two standalone packages, both of which are available at <https://github.com/wanxinjin/Pontryagin-Differentiable-Programming>. The video demos for some of the experiments are available at <https://wanxinjin.github.io/posts/pdp>.

E.1 System/Environment Setup

Quadrotor maneuvering control on $SE(3)$. We consider a quadrotor system maneuvering on $SE(3)$ space (i.e. full position and full attitude space). The equation of motion of a quadrotor is given by:

$$\begin{aligned} \dot{\mathbf{p}}_I &= \mathbf{v}_I, \\ m\dot{\mathbf{v}}_I &= m\mathbf{g}_I + \mathbf{f}_I, \\ \dot{\mathbf{q}}_{B/I} &= \frac{1}{2}\Omega(\omega_B)\mathbf{q}_{B/I}, \\ J_B\dot{\omega}_B &= \mathbf{M}_B - \omega \times J_B\omega_B. \end{aligned} \tag{S.13}$$

Here, the subscriptions $_B$ and $_I$ denote that a quantity is expressed in the quadrotor's body frame and inertial (world) frame, respectively; m is the mass of the quadrotor, respectively; $\mathbf{p} \in \mathbb{R}^3$ and $\mathbf{v} \in \mathbb{R}^3$ are the position and velocity vector of the quadrotor; $J_B \in \mathbb{R}^{3 \times 3}$ is the moment of inertia of the quadrotor with respect to its body frame; $\omega_B \in \mathbb{R}^3$ is the angular velocity of the quadrotor; $\mathbf{q}_{B/I} \in \mathbb{R}^4$ is the unit quaternion [75] describing the attitude of quadrotor with respect to the inertial frame; $\Omega(\omega_B)$ is

$$\Omega(\omega_B) = \begin{bmatrix} 0 & -\omega_x & -\omega_y & -\omega_z \\ \omega_x & 0 & \omega_z & -\omega_y \\ \omega_y & -\omega_z & 0 & \omega_x \\ \omega_z & \omega_y & -\omega_x & 0 \end{bmatrix} \tag{S.14}$$

and used for quaternion multiplication; $\mathbf{M}_B \in \mathbb{R}^3$ is the torque applied to the quadrotor; and $\mathbf{f}_I \in \mathbb{R}^3$ is the force vector applied to the quadrotor's center of mass (COM). The total force

magnitude $\|\mathbf{f}_I\| \in \mathbb{R}$ (along the z-axis of the body frame) and torque $\mathbf{M}_B = [M_x, M_y, M_z]$ are generated by thrusts $[T_1, T_2, T_3, T_4]$ of the four rotating propellers of the quadrotor, which can be written as

$$\begin{bmatrix} \|\mathbf{f}_I\| \\ M_x \\ M_y \\ M_z \end{bmatrix} = \begin{bmatrix} 1 & 1 & 1 & 1 \\ 0 & -l_w/2 & 0 & l_w/2 \\ -l_w/2 & 0 & l_w/2 & 0 \\ c & -c & c & -c \end{bmatrix} \begin{bmatrix} T_1 \\ T_2 \\ T_3 \\ T_4 \end{bmatrix}, \quad (\text{S.15})$$

with l_w being the wing length of the quadrotor and c a fixed constant.

We define the state and input vectors of the quadrotor system as

$$\mathbf{x} = [\mathbf{p}' \quad \mathbf{v}' \quad \mathbf{q}' \quad \boldsymbol{\omega}']' \in \mathbb{R}^{13} \quad \text{and} \quad \mathbf{u} = [T_1 \quad T_2 \quad T_3 \quad T_4]' \in \mathbb{R}^4. \quad (\text{S.16})$$

respectively. In design of the quadrotor's control objective function, to achieve $SE(3)$ maneuvering control performance, we need to carefully design the attitude error. As used in [76], we define the attitude error between the quadrotor's current attitude \mathbf{q} and the goal attitude \mathbf{q}_g as

$$e(\mathbf{q}, \mathbf{q}_g) = \frac{1}{2} \text{Tr}(\mathbf{I} - \mathbf{R}'(\mathbf{q}_g)\mathbf{R}(\mathbf{q})), \quad (\text{S.17})$$

where $\mathbf{R}(\mathbf{q}) \in \mathbb{R}^{3 \times 3}$ are the direction cosine matrix directly corresponding to \mathbf{q} (see [75] for more details). Other error term in the control objective is the distance to the respective goal:

$$e(\mathbf{p}, \mathbf{p}_g) = \|\mathbf{p} - \mathbf{p}_g\|^2, \quad e(\mathbf{v}, \mathbf{v}_g) = \|\mathbf{v} - \mathbf{v}_g\|^2, \quad e(\boldsymbol{\omega}, \boldsymbol{\omega}_g) = \|\boldsymbol{\omega} - \boldsymbol{\omega}_g\|^2. \quad (\text{S.18})$$

Two-link robot arm. The dynamics of a two-link robot arm can be found in [77, p. 171], where the state vector is $\mathbf{x} = [\mathbf{q}, \dot{\mathbf{q}}]'$ with $\mathbf{q} \in \mathbb{R}^2$ the vector of joint angles and $\dot{\mathbf{q}} \in \mathbb{R}^2$ the vector of joint angular velocities, and the control input $\mathbf{u} \in \mathbb{R}^2$ is the vector of torques applied to each joint.

Dynamics discretization. The continuous-time dynamics of all experimental systems in Table 2 are discretized using the Euler method: $\mathbf{x}_{t+1} = \mathbf{x}_t + \Delta \cdot \mathbf{f}(\mathbf{x}_t, \mathbf{u}_t)$ with the discretization interval $\Delta = 0.05\text{s}$ or $\Delta = 0.1\text{s}$.

Simulation environment source codes. We have made different simulation environments/systems in Table 2 as a standalone Python package, which is available at <https://github.com/wanxinjin/Pontryagin-Differentiable-Programming>. This environment package is easy to use and has user-friendly interfaces for customization.

E.2 Experiment of Imitation Learning

Data acquisition. The dataset of expert demonstrations $\{\boldsymbol{\xi}^d\}$ is generated by solving an expert optimal control system with the expert's dynamics and control objective parameter $\boldsymbol{\theta}^* = \{\boldsymbol{\theta}_{\text{dyn}}^*, \boldsymbol{\theta}_{\text{dyn}}^*\}$ given. We generate a number of five trajectories, where different trajectories $\boldsymbol{\xi}^d = \{\mathbf{x}_{0:T}^d, \mathbf{u}_{0:T-1}^d\}$ have different initial conditions \mathbf{x}_0 and time horizons T (T ranges from 40 to 50).

Inverse KKT method. We choose the inverse KKT method [52] for comparison because it is suitable for learning objective functions for high-dimensional continuous-space systems. We adapt the inverse KKT method, and define the KKT loss as the norm-2 violation of the KKT condition (S.11) by the demonstration data $\boldsymbol{\xi}^d$, that is,

$$\min_{\boldsymbol{\theta}, \boldsymbol{\lambda}_{1:T}} \left(\left\| \frac{\partial L}{\partial \mathbf{x}_{0:T}}(\mathbf{x}_{0:T}^d, \mathbf{u}_{0:T-1}^d) \right\|^2 + \left\| \frac{\partial L}{\partial \mathbf{u}_{0:T-1}}(\mathbf{x}_{0:T}^d, \mathbf{u}_{0:T-1}^d) \right\|^2 \right), \quad (\text{S.19})$$

where $\frac{\partial L}{\partial \mathbf{x}_{0:T}}(\cdot)$ and $\frac{\partial L}{\partial \mathbf{u}_{0:T-1}}(\cdot)$ are defined in (S.11) and $\boldsymbol{\theta} = \{\boldsymbol{\theta}_{\text{dyn}}, \boldsymbol{\theta}_{\text{dyn}}\}$. We minimize the above KKT-loss with respect to the unknown $\boldsymbol{\theta}$ and the costate variables $\boldsymbol{\lambda}_{1:T}$.

Note that to illustrate the inverse-KKT learning results in Fig. 3, we plot the imitation loss $L(\boldsymbol{\xi}_\theta, \boldsymbol{\theta}) = \|\boldsymbol{\xi}^d - \boldsymbol{\xi}_\theta\|^2$ instead of the KKT loss (S.19), because we want to guarantee that the comparison criterion is the same across different methods. Thus for each iteration k in minimizing the KKT loss (S.19), we use the parameter $\boldsymbol{\theta}_k$ to compute the optimal trajectory $\boldsymbol{\xi}_{\boldsymbol{\theta}_k}$ and obtain the imitation loss.

Neural policy cloning. For the neural policy cloning (similar to [78]), we directly learn a neural-network policy $\mathbf{u} = \pi_\theta(\mathbf{x})$ from the dataset using supervised learning, that is

$$\min_{\boldsymbol{\theta}} \sum_{t=0}^{T-1} \|\mathbf{u}_t^d - \pi_\theta(\mathbf{x}_t^d)\|^2. \quad (\text{S.20})$$

Learning neural control objective function. In Fig. 3d, we apply PDP to learn a neural objective function of the robot arm. The neural objective function is constructed as

$$J(\theta) = V_\theta(x) + 0.0001\|u\|^2, \quad (\text{S.21})$$

with $V_\theta(x)$ a fully-connected feed-forward network with n - n -1 layers and \tanh activation functions, i.e., an input layer with n neurons equal to the dimension of state, n , one hidden layer with n neurons and one output layer with 1 neuron. θ is the neural network parameter. We separate the input cost from the neural network because otherwise it will cause instability when solving OC problems in the forward pass. Also, in learning the above neural objective function, we fix the dynamics because otherwise it will also lead to instability of solving OC.

In the comparing GAIL method [56], we use the following hyper-parameters: the policy network is a fully-connected feed-forward network with n -400-300- m layers and relu activation functions; the discriminator network is a $(n+m)$ -400-300-1 fully-connected feed-forward network with \tanh and sigmoid activation functions; and the policy regularizer λ is set to zero.

Results and validation. In Fig. S1, we show more detailed results of imitation loss versus iteration for three systems (cart-pole, robot arm, and quadrotor). On each system, we run five trials for all methods with random initial guess, and the learning rate for all methods is set as $\eta = 10^{-4}$. In Fig. S4, we validate the learned models (i.e., learned dynamics and learned control objective) by performing motion planning of each system in unseen settings. Specifically, we set each system with new initial state x_0 and horizon T and plan the control trajectory using the learned models, and we also show the corresponding true trajectory of the expert.

E.3 Experiment of System Identification

Data acquisition. In the system identification experiment, we collect a total number of five trajectories from systems (in Table 2) with dynamics known, wherein different trajectories $\xi^o = \{x_{0:T}^o, u_{0:T-1}^o\}$ have different initial conditions x_0 and horizons T (T ranges from 10 to 20), with random inputs $u_{0:T-1}$ drawn from uniform distribution.

DMDc method. The DMDc method [57], which can be viewed as a variant of Koopman theory [6], estimates a linear dynamics model $x_{t+1} = Ax_t + Bu_t$, using the following least square regression

$$\min_{A,B} \sum_{t=0}^{T-1} \|x_{t+1}^o - Ax_t^o - Bu_t^o\|^2. \quad (\text{S.22})$$

Neural network baseline. For the neural network baseline, we use a neural network $f_\theta(x, u)$ to represent the system dynamics, where the input of the network is state and control vectors, and output is the state of next step. We train the neural network by minimizing the following residual

$$\min_{\theta} \sum_{t=0}^{T-1} \|x_{t+1}^o - f_\theta(x_t^o, u_t^o)\|^2. \quad (\text{S.23})$$

Learning neural dynamics model. In Fig. 4d, we compare the performance of PDP with Adam [58] for learning the same neural dynamics model for the robot arm system. Here, the neural dynamics model is a fully-connected feed-forward neural network with $(m+n)$ - $(2m+2n)$ - n layers and \tanh activation functions, that is, an input layer with $(m+n)$ neurons equal to the dimension of state, n , plus the dimension of control m , one hidden layer with $(2m+2n)$ neurons and one output layer with (n) neurons. The learning rate for the PDP and the PyTorch Adam is both set as $\eta = 10^{-5}$.

Results and validation. In Fig. S2, we show more detailed results of SysID loss versus iteration for the three systems (cart-pole, robot arm, and quadrotor). On each system, we run five trials with random initial guess, and we set the learning rate as $\eta = 10^{-4}$ for all methods. In Fig. S5, we use the learned dynamics model to perform motion prediction of each system in unactuated conditions (i.e., $u_t = 0$), in order to validate the effectiveness/correctness of the learned dynamics models.

E.4 Experiment of Control/Planning

We use the dynamics identified in the system ID part, and the specified control objective function is set as weighted distance to the goal, as given in Table 2 (θ_{obj} is given). Throughout the optimal control/planning experiments, we use the time horizons T ranging from 20 to 40.

Learning neural network policies. On the cart-pole and robot-arm systems (in Fig. 5a and Fig. 5b), we learn a feedback policy by minimizing given control objective functions. For both systems, we parameterize the policy using a neural network. Specifically, we use a fully-connected feed-forward neural network which has a layer structure of n - n - m with \tanh activation functions, i.e., there is an input layer with n neurons equal to the dimension of state, one hidden layer with n neurons and one output layer with m neurons. The policy parameter θ is the neural network parameter. We apply the PDP Control/Planning mode in Algorithm 5 and set the learning rate $\eta = 10^{-4}$. For comparison, we apply the guided policy search (GPS) method [59] (its deterministic version) to learn the same neural policy with the learning rate $\eta = 10^{-6}$ (η in GPS is used to update the Lagrange multipliers for the policy constraint and we choose $\eta = 10^{-6}$ because it achieves the most stable results).

Motion planning with Lagrange polynomial policies. On the 6-DoF quadrotor, we use PDP to perform motion planning, that is, to find a control sequence to minimize the given control cost (loss) function. Here, we parameterize the policy $\mathbf{u}_t = \mathbf{u}(t, \theta)$ as N -degree Lagrange polynomial [80] with $N + 1$ pivot points evenly populated over the time horizon, that is, $\{(t_0, \mathbf{u}_0), (t_1, \mathbf{u}_1), \dots, (t_N, \mathbf{u}_N)\}$ with $t_i = iT/N, i = 0, \dots, N$. The analytical form of the parameterized policy is

$$\mathbf{u}(t, \theta) = \sum_{i=0}^N \mathbf{u}_i b_i(t) \quad \text{with} \quad b_i(t) = \prod_{0 \leq j \leq N, j \neq i} \frac{t - t_j}{t_i - t_j}. \quad (\text{S.24})$$

Here, $b_i(t)$ is called Lagrange basis, and the policy parameter θ is defined as

$$\theta = [\mathbf{u}_0, \dots, \mathbf{u}_N]' \in \mathbb{R}^{m(N+1)}. \quad (\text{S.25})$$

The above Lagrange polynomial parameterization has been normally used in some trajectory optimization method such as [41, 81]. In this planning experiment, we have used different degrees of Lagrange polynomials, i.e., $N = 5$ and $N = 35$, respectively, to show how policy expressiveness can influence the final control loss (cost). The learning rate in PDP is set as $\eta = 10^{-4}$. For comparison, we also apply iLQR [38] to solve for the optimal control sequence.

Results In Fig. S3, we show the detailed results of control loss (i.e. the value of control objective function) versus iteration for three systems (cart-pole, robot arm, and quadrotor). For each system, we run five trials with random initial parameter θ_0 . In Fig. S6, we apply the learned neural network policies (for cart-pole and robot arm systems) and the Lagrange polynomial policy (for quadrotor system) to simulate the corresponding system. For reference, we also plot the optimal trajectory solved by an OC solver [79] (which corresponds to the minimal control cost).

Comments on the result comparison between GPS [59] and PDP. In learning feedback policies, comparing the results obtained by the guided policy search (GPS) [59] and PDP in Fig. S3 and in Fig. S6, we have the following remarks.

(1) PDP outperforms GPS in terms of having lower control loss (cost). This can be seen in Fig. S3 and Fig. S6 (in Fig. S6, PDP results in a simulated trajectory which is closer to the optimal one than that of GPS). This can be understood from the fact that GPS considers the policy as constraint and updates it in a supervised learning step during the learning process. Although GPS aims to *simultaneously* minimize the control cost and the degree to which the policy is violated, it does not necessarily mean that before the learning researches convergence, when *strictly following* a pre-convergence control policy, the system will have a cost as minimal as it can possibly achieve.

(2) Instead, PDP adopts a different way to synchronize the fulfillment of policy constraints and the minimization of the control cost. In fact, throughout the entire learning process, PDP always guarantees that the policy constraint is perfectly respected (as the forward pass strictly follows the policy). Therefore, the core difference between PDP and GPS is that PDP does not simultaneously minimize two aspects—the policy violation and control cost, instead, it enforces that one aspect—policy—is always respected and only focuses on minimizing the other—control cost. The benefit of doing so is that at each learning step, the control cost for PDP is always as minimal as it can possibly achieve. This explains why PDP outperforms GPS in terms of having lower control cost (loss).

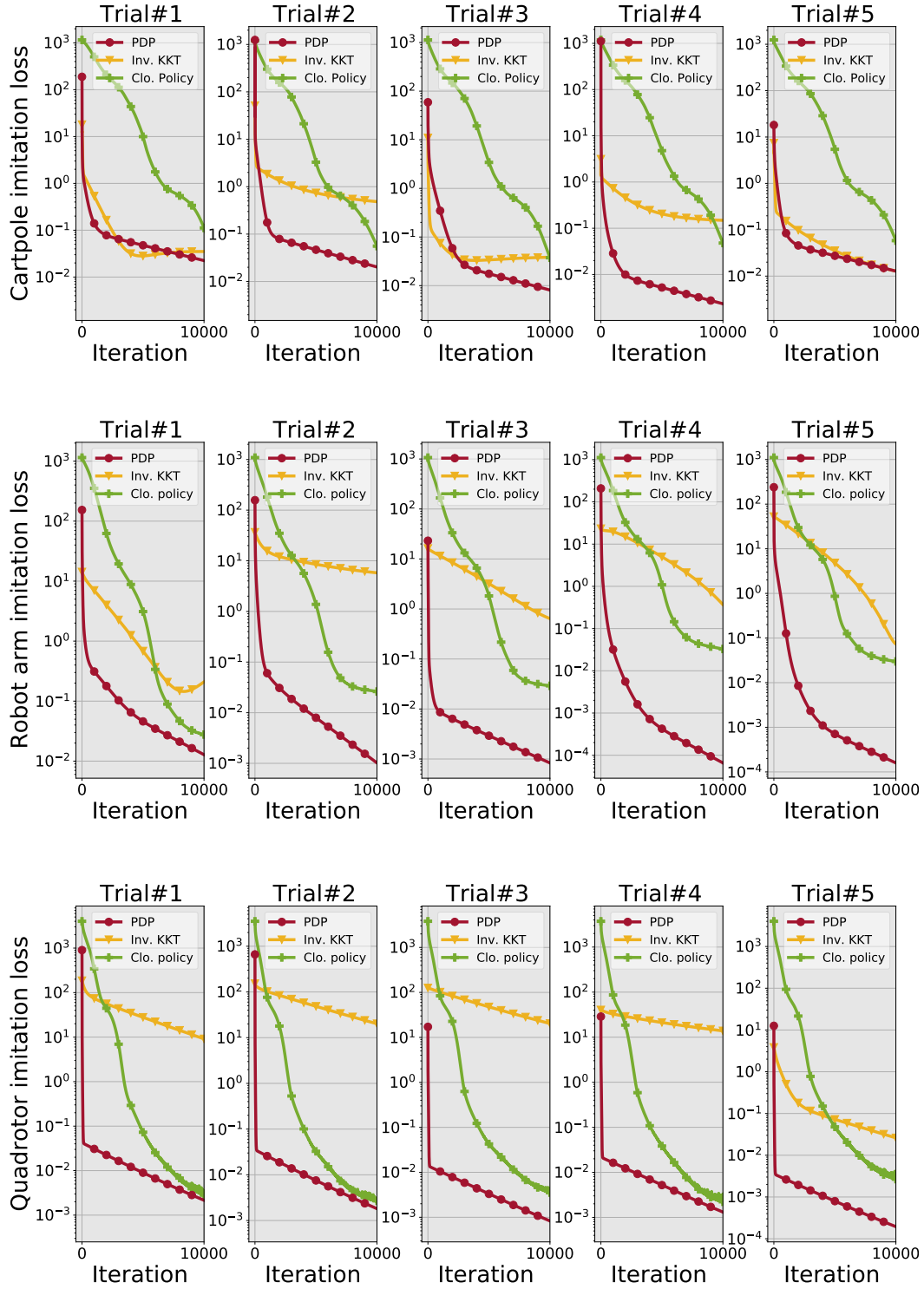


Figure S1: Experiments for PDP IRL/IOC Mode: imitation loss versus iteration. For each system, we run five trials starting with random initial guess θ_0 , and the learning rate is $\eta = 10^{-4}$ for all methods. The results show a significant advantage of the PDP over the neural policy cloning and inverse-KKT [52] in terms of lower training loss and faster convergence speed. Please see Appendix Fig. S4 for validation. Please find the video demo at <https://youtu.be/awVNiCIJCfs>.

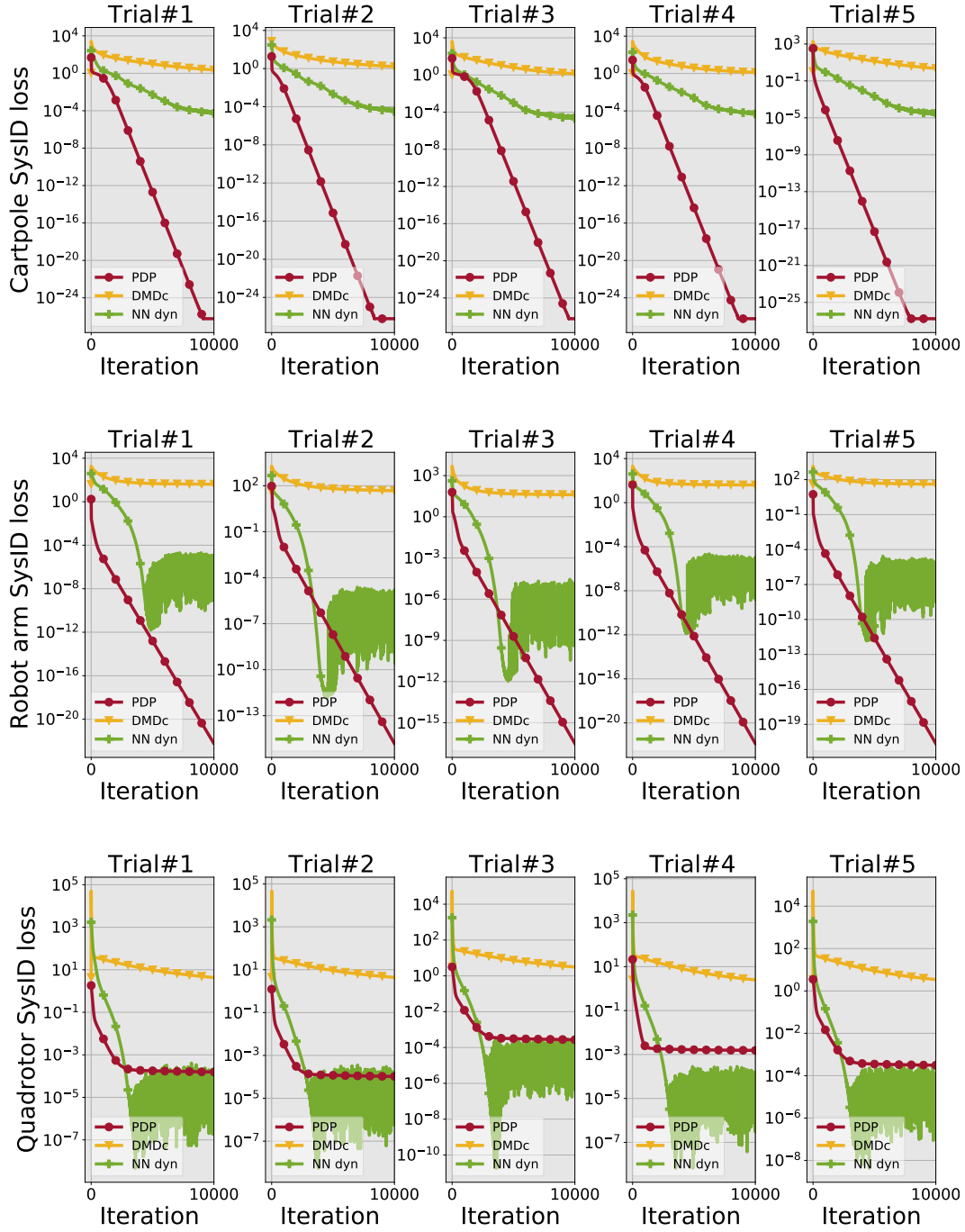


Figure S2: Experiments for PDP SysID Mode: SysID loss versus iteration. For each system, we run five trials with random initial guess θ_0 , and set the learning rate $\eta = 10^{-4}$ for all methods. The results show a significant advantage of the PDP over neural-network dynamics and DMDc in terms of lower training loss and faster convergence speed. Please see Fig. S5 for validation. Please find the video demo at <https://youtu.be/PayBZjDD60Y>.

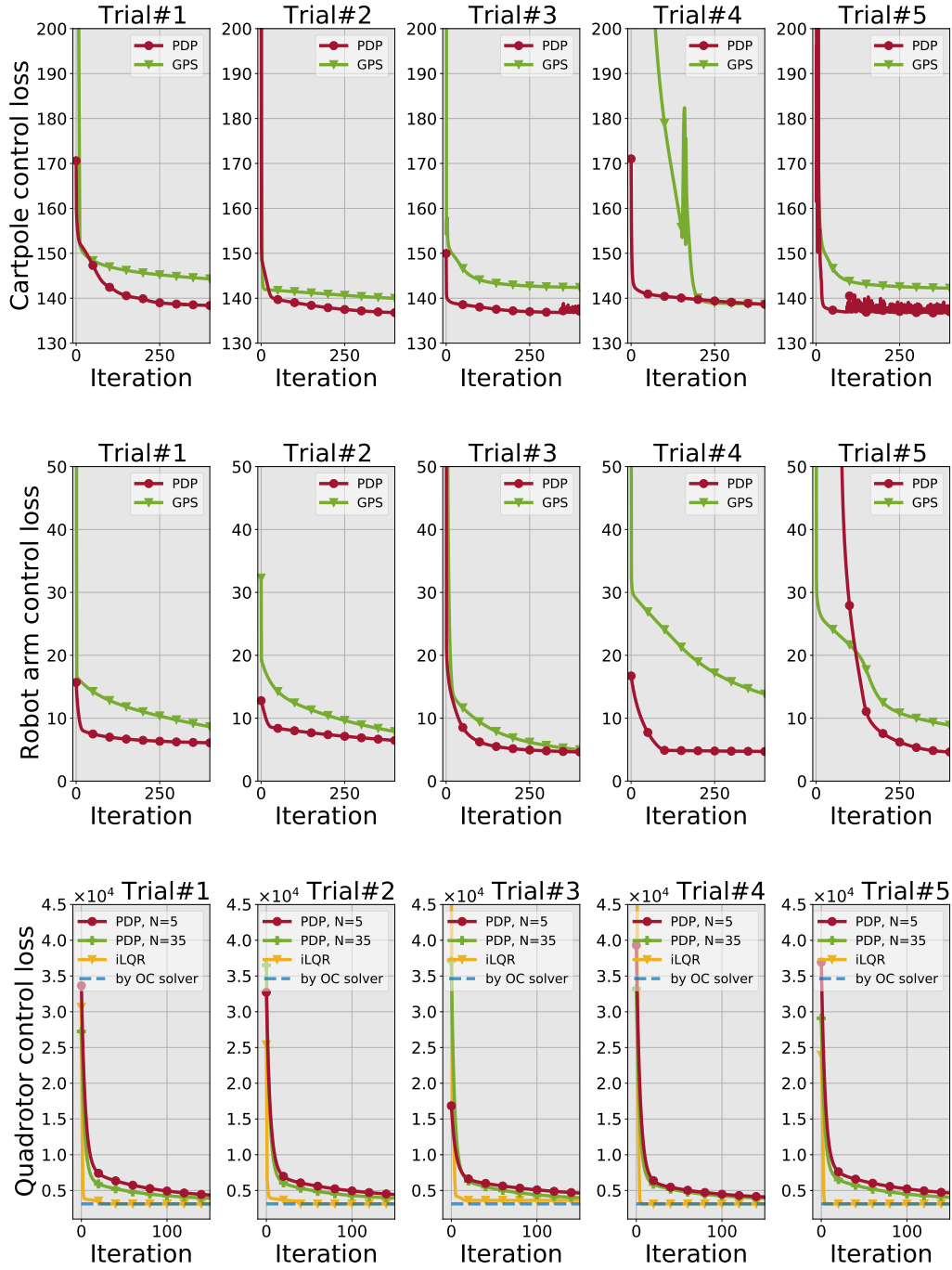


Figure S3: Experiments for PDP Control/Planning Mode: control loss (i.e., objective function value) versus iteration. For the cart-pole (top panel) and robot arm (middle panel) systems, we learn neural feedback policies, and compare with the GPS method [59]. For the quadrotor system, we perform motion planning with a Lagrange polynomial policy (we use different degree N), and compare with iLQR and an OC solver [79]. The results show that for learning feedback control policies, PDP outperforms GPS in terms of having lower control loss (cost); and for motion planning, iLQR has faster convergence speed than PDP. Please find the video demo at <https://youtu.be/KTw6TAigfPY>.

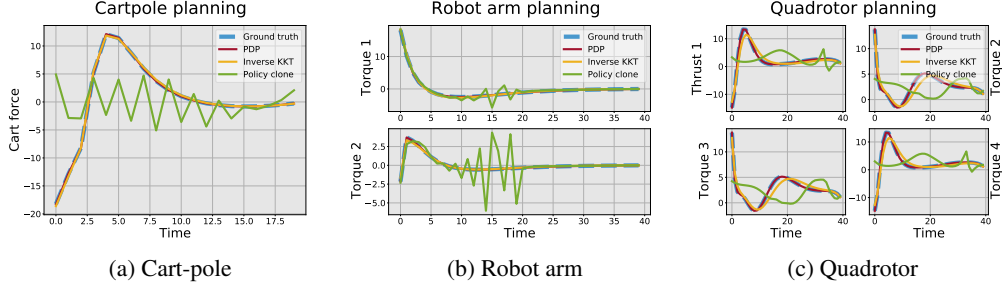


Figure S4: Validation for the imitation learning experiment in Fig. S1. We preform motion planing for each system in unseen conditions (new initial condition and new time horizon) using the learned models. Results show that compared to the neural policy cloning and inverse KKT [52], PDP result can accurately plan the expert’s trajectory in unseen settings. This indicates PDP can accurately learn the dynamics and control objective, and has the better generality than the other two. Although policy imitation has lower imitation loss than inverse KKT, it has the poorer performance in planing. This is because with limited data, the cloned policy can be over-fitting, while the inverse KKT learns a cost function, a high-level representation of policies, thus has better generality to unseen conditions.

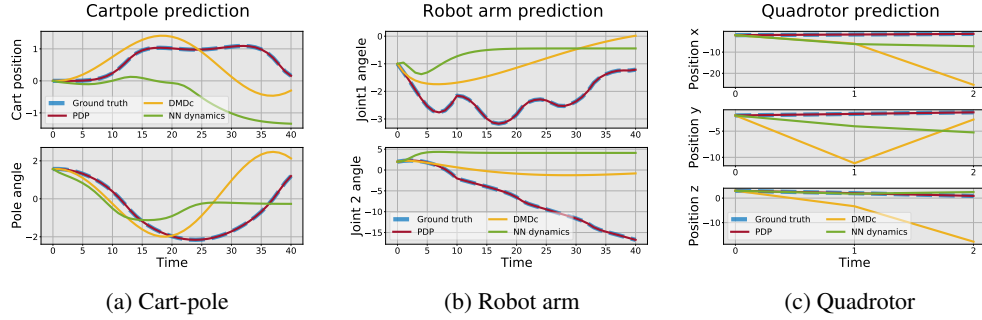


Figure S5: Validation for the system identification experiment in Fig. S2. We perform motion prediction in unactuated conditions ($u = 0$) using the learned dynamics. Results show that compared to neural-network dynamics training and DMDC, PDP can accurately predict the motion trajectory of each systems. This indicates the effectiveness of the PDP in identifying dynamics models.

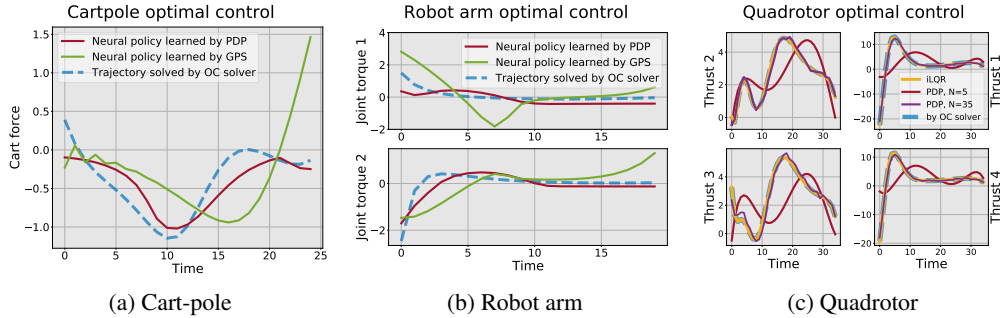


Figure S6: Simulation of the learned policies in the control and planning experiment in Fig. S3. Fig. S6a-S6b are the simulations of the learned neural feedback policies on the cart-pole and robot arm systems, respectively, where we also plot the optimal trajectory solved by an OC solver [79] for reference. From Fig. S6a-S6b, we observe that PDP results in a trajectory that is much closer to the optimal one than that of GPS; this implies that PDP has lower control loss (please check our analysis on this in Appendix E.4) than GPS. Fig. S6c is the planning results for the quadrotor system using PDP, iLQR, and an OC solver [79], where we have used different degrees of Lagrange polynomial policies in PDP. The results show that PDP can successfully plan a trajectory very close to the ground truth optimal trajectory. We also observe that the accuracy of the resulting trajectory depends on choice of the policy parameterization (i.e., expressive power): for example, the use of polynomial policy of a higher degree N results in a trajectory closer to the optimal one (the one using the OC solver) than the use of a lower degree. iLQR is generally able to achieve high-accuracy solutions because it directly optimizes the loss function with respect to individual control inputs (instead of a parameterized policy), but this comes at the cost of high computation expense, as shown in Fig. 5d.

F Related End-to-End Learning Frameworks

As discussed in Section 7, two categories are related to this work. Here, we only detail the difference of PDP from the second category, i.e., the methods that learn an implicit planner within a RL policy.

Differentiable MPC. [67] develops an end-to-end differentiable MPC framework to jointly learn the system dynamics model and control objective function of an optimal control system. In the forward pass, it first uses iLQR [38] to solve the optimal control system and find a fixed point, and then approximate the optimal control system by a LQR at the fixed point. In the backward pass, the gradient is obtained by differentiating the LQR approximation. This process, however, may have two drawbacks: first, since the differentiation in the backward pass is conducted on the LQR approximation instead of on the original system, the obtained gradient thus may not be accurate due to discrepancy of approximation; and second, computing the gradient of the LQR approximation requires the inverse of a coefficient matrix, whose size is $(2n + m)T \times (2n + m)T$ with n and m state and action dimensions, respectively, T the time horizon of the OC system, thus this will cause huge computational cost when handling the system of longer time horizon T .

Compared to differentiable MPC, the first advantage of the PDP framework is that the differentiation in the backward pass is directly performed on the parameterized optimal control system (by differentiating through PMP). Second, we develop the auxiliary control system in the backward pass of PDP, whose trajectory is exactly the gradient of the system trajectory in the forward pass. The gradient then is iteratively solved using the auxiliary control system by Lemma 5.2 (Algorithm 2). Those proposed techniques enable the PDP to have significant advantage in computational efficiency over differentiable MPC. To illustrate this, we have compared the algorithm complexity for both PDP and differentiable MPC in Table S1 and provide an experiment in Fig. S7.

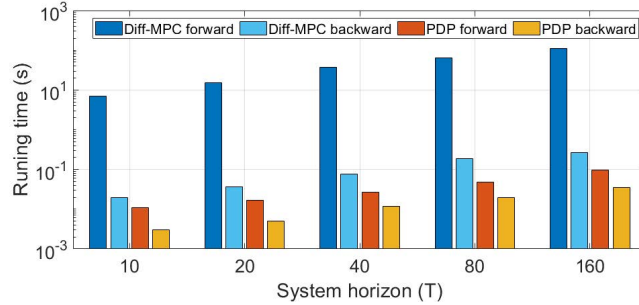


Figure S7: Runtime (per iteration) comparison between the PDP and differentiable MPC [67] for different time horizons of a pendulum system. Note that y-axis is log-scale, and the runtime is averaged over 100 iterations. Both methods are implemented in Python and run on the same machine using CPUs. The results show that the PDP runs 1000x faster than differentiable MPC.

Path Integral Network. [65] and [66] develop a differentiable end-to-end framework to learn path-integral optimal control systems. Path-integral optimal control systems [69] however are a limited category of optimal control systems, where the dynamics is affine in control input and the control objective function is quadratic in control input. More differently, this path integral network is essentially an ‘unrolling’ method, which means that the forward pass of solving optimal control is extended as a graph of multiple steps of applying gradient descent, and the solution of the optimal control system is considered as the output of the final step of the gradient descent operations. Although the advantage of this unrolling (gradient descent) computational graph is that it can immediately take advantage of automatic differentiation techniques such as TensorFlow [70] to obtain the gradient in backpropagation, its drawback is however obvious: the framework is both memory- and computationally- expensive because it needs to store and traverse all intermediate results of the gradient descent process along the graph; furthermore, there is a conflict between computational complexity and accuracy in the forward pass. We have provided its complexity analysis in Table S1.

Universal Planning Network. In [68], the authors develop an end-to-end imitation learning framework consisting of two layers: the inner layer is a planner, which is formulated as an optimal control system in a latent space and is solved by gradient descent, and an outer layer to minimize the imitation

loss between the output of inner layer and expert demonstrations. However, this framework is also based on the ‘unrolling’ strategy. Specifically, the inner planning layer using gradient descent is considered as a large computation graph, which chains together the sub-graphs of each step of gradient descent. In the backward pass, the gradient derived from the outer layer back-propagates through the entire computation graph. Again, this unrolled learning strategy will incur huge memory and computation costs in implementation. Please find its complexity analysis in Table S1.

Different from the above ‘unrolling’ learning methods [65, 66, 68, 82], the proposed PDP method handles the learning of optimal control systems in a ‘direct and compact’ manner. Specifically, in forward pass, PDP only obtains and stores the final solution of the optimal control system and does not care about the (intermediate) process of how such solution is obtained. Thus, the forward pass of the PDP accepts any external optimal control solver such as CasADi [79]. Using the solution in the forward pass, the PDP then automatically builds the auxiliary control system, based on which, the exact *analytical* gradient is solved efficiently in backward pass. Such features guarantee that the complexity of the PDP framework is only linearly scaled up to the time horizon of the system, which is significantly efficient than the above ‘unrolling’ learning methods (please find the comparison in Table S1). In Appendix G, we will present the detailed complexity analysis.

Table S1: Complexity comparison for different end-to-end learning frameworks

Learning frameworks	Forward pass		Backward pass	
	Method and accuracy	Complexity (linear to)	Method	Complexity (linear to)
PI-Net [65]	N -step unrolled graph using gradient descent; accuracy depends on N	computation: NT memory: NT	Back-propagation over the unrolled graph	computation: NT memory: NT
UPN [68]	N -step unrolled graph using gradient descent; accuracy depends on N	computation: NT memory: NT	Back-propagation over the unrolled graph	computation: NT memory: NT
Diff-MPC [67]	iLQR finds fixed points; can achieve any accuracy	computation: — memory: T	Differentiate the LQR approximation and solve linear equations	computation: T^2 memory: T^2
PDP	Accept any OC solver; can achieve any accuracy	computation: —, memory: T	Auxiliary control system	computation: T , memory: T

*Here T denotes the time horizon of the system;

G Complexity of PDP

We consider the algorithm complexity of different learning modes of PDP (see Appendix D), and suppose that the time horizon of the parameterized system $\Sigma(\theta)$ is T .

IRL/IOC Mode (Algorithm 3): in forward pass, PDP needs to obtain and store the optimal trajectory ξ_θ of the optimal control system $\Sigma(\theta)$ in (1), and this optimal trajectory can be solved by any (external) optimal control solver. In backward pass, PDP first uses ξ_θ to build the auxiliary control system $\bar{\Sigma}(\xi_\theta)$ in (16) and then computes $\frac{\partial \xi_\theta}{\partial \theta}$ by Lemma 5.2, which takes $2T$ steps.

SysID Mode (Algorithm 4): in forward pass, PDP needs to obtain and store the trajectory ξ_θ of the original dynamics system $\Sigma(\theta)$ in (5). Such trajectory is simply a result of iterative integration of (5), which takes T steps. In backward pass, PDP first uses ξ_θ to build the auxiliary control system $\bar{\Sigma}(\xi_\theta)$ in (20) and then computes $\frac{\partial \xi_\theta}{\partial \theta}$ by iterative integration of (20), which takes T steps.

Control/Planning Mode (Algorithm 5): in forward pass, PDP needs to obtain and store the trajectory ξ_θ of the controlled system $\Sigma(\theta)$ in (7). Such trajectory is simply a result of iterative integration of (7), which takes T steps. In backward pass, PDP first uses ξ_θ to build an auxiliary control system $\bar{\Sigma}(\xi_\theta)$ in (21) and then computes $\frac{\partial \xi_\theta}{\partial \theta}$ by integration of (21), which takes T steps.

Therefore, we can summarize that the memory- and computational- complexity for the PDP framework is only linear to the time horizon T of the parameterized system $\Sigma(\theta)$. This is significantly advantageous over existing end-to-end learning frameworks, as summarized in Table S1.

H Limitation of PDP

PDP is a first-order algorithm. We observe that (i) all gradient quantities in PDP are analytical and exact; (ii) the development of PDP does not involve any second-order derivative/approximation of functions or models (note that PMP is a first-order optimality condition for optimal control); and (iii) PDP minimizes a loss function directly with respect to unknown parameters in a system using gradient descent. Thus, we conclude that PDP is a first-order gradient-descent based optimization framework. Specifically for the SysID and Control/Planning modes of PDP, they are also first-order algorithms. When using these modes to solve optimal control problems, this first-order nature may bring disadvantages of PDP compared to high-order methods, such as iLQR which can be considered as 1.5-order because it uses second-order derivative of a value function and first-order derivative of dynamics, or DDP which is a second-order method as it uses the second-order derivatives of both value function and dynamics. The disadvantages of PDP have already been empirically shown in Fig. 5c and Fig. S3, where the converging speed of PDP in its planning mode is slower than that of iLQR. For empirical comparisons between first- and second-order techniques, we refer the reader to [83].

Convergence to local minima. *Since PDP is a first-order gradient-descent based algorithm, PDP can only achieve local minima for general non-convex optimization problems in (3).* Furthermore, we observe that the general problem in (3) belongs to a bi-level optimization framework. As explored in [71], under certain assumptions such as convexity and smoothness on models (e.g., dynamics model, policy, loss function and control objective function), global convergence of the bi-level optimization can be established. But we think such conditions are too restrictive in the context of dynamical control systems. As a future direction, we will investigate mild conditions for good convergence by resorting to dynamical system and control theory, such as Lyapunov theory.

Parameterization matters for global convergence. Although PDP only achieves local convergence, these still exists a question of how likely PDP can obtain the global convergence. In our empirical experiments, we find that how models are parameterized matters for good convergence performance. For example, in IOC/IRL mode, we observe that using a neural network control objective function (in Fig. 3d) is more likely to get trapped in local minima than using the parameterization of weighted distance objective functions (in Fig. 3a-3c). In control/planning mode, using a deeper neural network policy (in Fig. 5a-5b) is more like to result in local minima than using a simpler one. Also in the motion planning experiment, we use the Lagrange polynomial to parameterize a policy instead of using standard polynomials, because the latter can lead to poor conditioning and sensitivity issues (a small change of polynomial parameter results in large change in performance) and thus more easily get stuck in local minima. One high-level explanation is that more complex parameterization will bring extreme non-convexity to the optimization problem, making the algorithm more easily trapped in local minima. Again, how to theoretically justify those empirical experience and find the mild conditions for global convergence guarantee still needs to be investigated in future research.

I PDP to Solve 6-DoF Rocket Powered Landing Problems

As a final part in this supplementary, we will demonstrate the capability of PDP to solve the more challenging 6-DoF rocket powered landing problems.

We here omit the description of mechanics modeling for the 6-DoF powered rocket system, and refer the reader to Page 5 in [84] for the rigid body dynamics model of a rocket system (the notations and coordinates used below follows the ones in [84]). The state vector of the rocket system is defined as

$$\mathbf{x} = [m \quad \mathbf{r}'_{\mathcal{I}} \quad \mathbf{v}'_{\mathcal{I}} \quad \mathbf{q}'_{\mathcal{B}/\mathcal{I}} \quad \boldsymbol{\omega}'_{\mathcal{B}}]' \in \mathbb{R}^{14}, \quad (\text{S.26})$$

where $m \in \mathbb{R}$ is the mass of the rocket; $\mathbf{r}_{\mathcal{I}} \in \mathbb{R}^3$ and $\mathbf{v}_{\mathcal{I}} \in \mathbb{R}^3$ are the position and velocity of the rocket (center of mass) in the inertially-fixed Up-East-North coordinate frame; $\mathbf{q}_{\mathcal{B}/\mathcal{I}} \in \mathbb{R}^4$ is the unit quaternion denoting the attitude of rocket body frame with respect to the inertial frame (also see the description in the quadrotor dynamics in Appendix E.1); and $\boldsymbol{\omega}_{\mathcal{B}} \in \mathbb{R}^3$ is the angular velocity of the rocket expressed in the rocket body frame. In our simulation, we only focus on the final descending phase before landing, and thus assume the mass depletion during such a short phase is very slow and thus $\dot{m} \approx 0$. We define the control input vector of the rocket, which is the thrust force vector

$$\mathbf{u} = \mathbf{T}_{\mathcal{B}} = [T_x, T_y, T_z]' \in \mathbb{R}^3, \quad (\text{S.27})$$

acting on the gimbal point of the engine (situated at the tail of the rocket) and is expressed in the body frame. Note that the relationship between the total torque \mathbf{M}_B applied to the rocket and the thrust force vector \mathbf{T}_B is $\mathbf{M}_B = \mathbf{r}_{T,B} \times \mathbf{T}_B$, with $\mathbf{r}_{T,B} \in \mathbb{R}^3$ being constant position vector from the center-of-mass of the rocket to the gimbal point of the engine. The continuous dynamics is discretized using the Euler method: $\mathbf{x}_{t+1} = \mathbf{x}_t + \Delta \cdot \mathbf{f}(\mathbf{x}_t, \mathbf{u}_t)$ with the discretization interval $\Delta = 0.1s$.

For the rocket system, the unknown dynamics parameter, $\boldsymbol{\theta}_{\text{dyn}}$, includes the rocket's initial mass m_0 , and the moment of inertia $\mathbf{J}_B \in \mathbb{R}^{3 \times 3}$, and the rocket length ℓ , thus, $\boldsymbol{\theta}_{\text{dyn}} = \{m_0, \mathbf{J}_B, \ell\} \in \mathbb{R}^8$.

For the control objective (cost) function, we consider a weighted combination of the following aspects:

- distance of the rocket position from the target position, associated with weight w_1 ;
- distance of the rocket velocity from the target velocity, associated with weight w_2 ;
- penalty of the excessive title angle of the rocket, associated with weight w_3 ;
- penalty of the side effects of the thrust vector, associated with weight w_4 ;
- penalty of the total fuel cost, associated with weighted w_5 .

So the parameter of the control objective function, $\boldsymbol{\theta}_{\text{obj}} = [w_1, w_2, w_3, w_4, w_5]^\top \in \mathbb{R}^5$. In sum, the overall parameter for the 6-DoF rocket powered landing control system is

$$\boldsymbol{\theta} = \{\boldsymbol{\theta}_{\text{dyn}}, \boldsymbol{\theta}_{\text{obj}}\} \in \mathbb{R}^{13}. \quad (\text{S.28})$$

Imitation learning. We apply the IRL/IOC mode of PDP to perform imitation learning of the 6-DoF rocket powered landing. The experiment process is similar to the experiments in Appendix E.2, where we collect five trajectories from an expert system with dynamics and control objective function both known (different trajectories have different time horizons T ranging from 40 to 50 and different initial state conditions). Here we minimize imitation loss $L(\boldsymbol{\xi}_\theta, \boldsymbol{\theta}) = \|\boldsymbol{\xi}^d - \boldsymbol{\xi}_\theta\|^2$ over the parameter of dynamics and control objective, $\boldsymbol{\theta}$ in (S.28). The learning rate is set to $\eta = 10^{-4}$, and we run five trials with random initial parameter guess $\boldsymbol{\theta}_0$. The imitation loss $L(\boldsymbol{\xi}_\theta, \boldsymbol{\theta})$ versus iteration is plotted in Fig. S8a. To validate the learned models (the learned dynamics and the learned objective function), we use the learned models to perform motion planing of rocket powered landing in unseen settings (here we use new initial condition and new time horizon). The planing results are plotted in Fig. S8b, where we also plot the ground truth for comparison.

System identification. We apply the SysID mode of PDP to identify the dynamics parameter $\boldsymbol{\theta}_{\text{dyn}}$ of the rocket. The experiment process is similar to the experiments in Appendix E.3, where we collect five trajectories with different initial state conditions, time horizons (T ranges from 10 to 20), and random control inputs. We minimize the SysID loss $L(\boldsymbol{\xi}_\theta, \boldsymbol{\theta}) = \|\boldsymbol{\xi}^o - \boldsymbol{\xi}_\theta\|^2$ over $\boldsymbol{\theta}_{\text{dyn}}$ in (S.28). The learning rate is set to $\eta = 10^{-4}$, and we run five trials with random initial parameter guess for $\boldsymbol{\theta}_{\text{dyn}}$. The SysID loss $L(\boldsymbol{\xi}_\theta, \boldsymbol{\theta})$ versus iteration is plotted in Fig. S9a. To validate the learned dynamics, we use it to predict the motion of rocket given a new sequence of control inputs. The prediction results are in Fig. S9b, where we also plot the ground truth for reference.

Optimal powered landing control. We apply the Control/Planning mode of PDP to find an optimal control sequence for the rocket to perform a successful powered landing. The experiment process is similar to the experiments performed for the quadrotor system in Appendix E.4. We set the time horizon as $T = 50$, and randomly choose an initial state condition \mathbf{x}_0 for the rocket. We minimize the control loss function, which is now a given control objective function with $\boldsymbol{\theta}_{\text{obj}}$ known. The control policy we use here is parameterized as the Lagrangian polynomial, as described in (S.24) in Appendix E.4, here with degree $N = 25$. The control loss is set as the control objective function learned in the previous imitation learning experiment. The learning rate is set to $\eta = 10^{-4}$, and we run five trials with random initial guess of the policy parameter. The the control loss $L(\boldsymbol{\xi}_\theta, \boldsymbol{\theta})$ versus iteration is plotted in Fig. S10a. To validate the learned optimal control policy, we use it to simulate the motion (control trajectory) of the rocket landing, and compare with the ground truth optimal trajectory obtained by an OC solver. The validation results are in Fig. S10b.

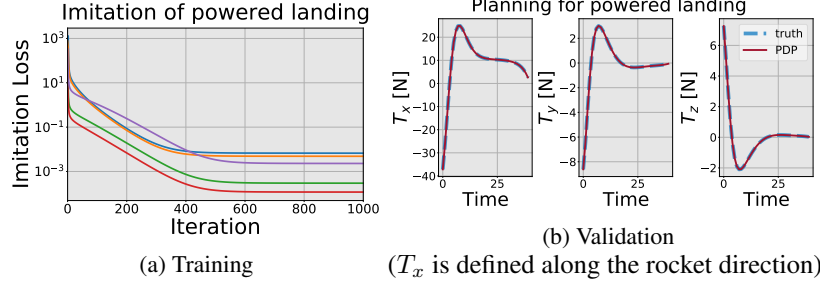


Figure S8: (a) Training process for imitation learning of 6-DoF rocket powered landing: the imitation loss versus iteration; here we have performed five trials (labeled by different colors) with random initial parameter guess. (b) Validation: we use the learned models (dynamics and control objective function) to perform motion planning of the rocket powered landing in unseen settings (i.e. given new initial state condition and new time horizon requirement); here we also plot the ground-truth motion planning of the expert for reference. The results in (a) and (b) show that the PDP can accurately learn the dynamics and control objective function from demonstrations, and have good generalizability to novel situations. Please find the video demo at <https://youtu.be/4RxDLxUcMp4>.

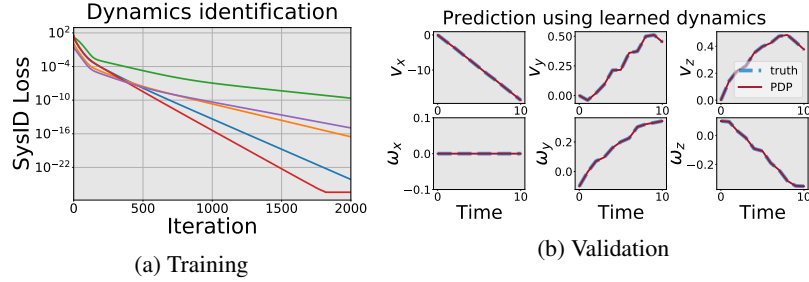


Figure S9: (a) Training process for identification of rocket dynamics: SysID loss versus iteration; here we have performed five trials (labeled by different colors) with random initial parameter guess. (b) Validation: we use the learned dynamics model to perform motion prediction of the rocket given a new control sequence; here we also plot the ground-truth motion (where we know the exact dynamics). The results in (a) and (b) show that the PDP can accurately identify the dynamics model of the rocket.

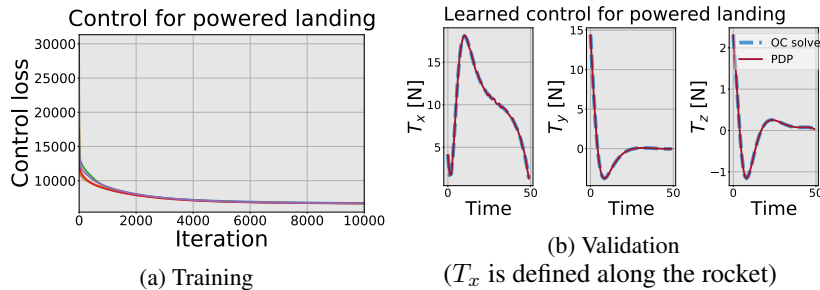


Figure S10: (a) Training process of learning the optimal control policy for rocket powered landing: the control loss versus iteration; here we have performed five trials (labeled by different colors) with random initial guess of the policy parameter. (b) Validation: we use the learned policy to simulate the rocket control trajectory; here we also plot the ground-truth optimal control solved by an OC solver. The results in (a) and (b) show that the PDP can successfully find the optimal control policy (or optimal control sequence) to successfully perform the rocket powered landing. Please find the video demo at <https://youtu.be/5Jsu772Sqcg>.